INTERIM REPORT

Evaluating the Integrity of the Ogallala Fine-Grained Zone Using Airborne Geophysics

by Jeffrey G. Paine

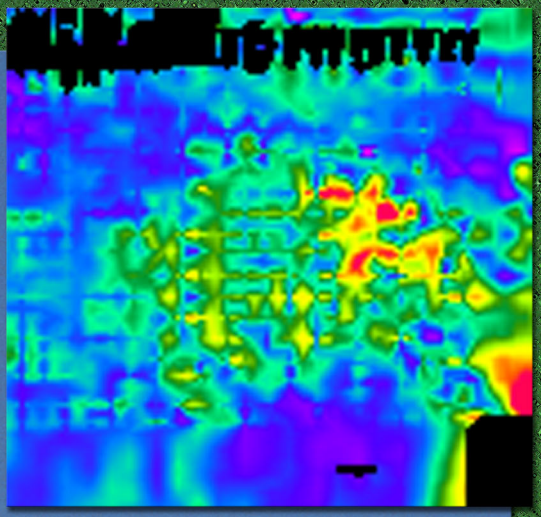

Prepared for

BWXT Pantex
P.O. Box 30020
Pantex Plant
Amarillo, Texas 79120-0020

Contract no. 00026424

Bureau of Economic Geology
Scott W. Tinker, Director
John A. and Katherine G. Jackson School of Geosciences
The University of Texas at Austin
Austin, Texas 78713-8924

October 2003

INTERIM REPORT

EVALUATING THE INTEGRITY OF THE OGALLALA FINE-GRAINED ZONE USING AIRBORNE GEOPHYSICS

by

Jeffrey G. Paine
Bureau of Economic Geology
The University of Texas at Austin

Mail address:
University Station, Box X
Austin, Texas 78713-8924

Street address:
J. J. Pickle Research Campus, Building 130
10100 Burnet Road
Austin, Texas 78758-4445
jeff.paine@beg.utexas.edu

Interim report prepared for

BWXT Pantex
P.O. Box 30020
Pantex Plant
Amarillo, Texas 79120-0020

Contract No. 00026424

October 2003

Page intentionally blank

CONTENTS

FIGURES

TABLES

SUMMARY

This interim report summarizes results to date from the March 2003 airborne geophysical survey of the Pantex Plant. This survey was completed to investigate the potential for lateral and vertical migration of groundwater in the perched aquifer and assess the integrity of the Ogallala fine-grained zone (FGZ) that perches groundwater above the Ogallala aquifer at the Pantex Plant. Airborne geophysical instruments acquired time-domain electromagnetic induction (TDEM) data along flight lines totaling 1,243 km in length within four survey blocks located north, east, south, and west of the main Pantex Plant. TDEM data were processed to produce profiles of apparent conductivity variations with depth at more than 100,000 locations within the survey blocks. Measurements with excessive noise were filtered from the final data set. We used the remaining apparent conductivity profiles to produce survey-wide and local-area depth slices depicting apparent conductivity changes at 10-m depth intervals between 10- and 200-m depth. These depths are sufficient to examine apparent conductivity patterns and associated hydrological and geological characteristics of the upper Ogallala unsaturated zone above the perched aquifer, the perched aquifer and FGZ, the zone below the FGZ and above the Ogallala water table, the lower Ogallala Formation, and in places pre-Ogallala strata. In addition to survey-wide conductivity data, we have extracted site-specific data for focused investigations at Playa 3, the old Sewage Treatment Plant (OSTP), and in the Pantex Southeast plume area.

Geological and hydrological data available from numerous wells and borings have yet to be integrated into the geophysical data set. Geological and hydrological interpretations made in this report are preliminary pending more complete analysis using available subsurface data. Interpretations to date are based on geophysical data alone and may change as geologic, hydrologic, and geophysical data are integrated. Preliminary results include the observation that the conductivity structure beneath surveyed playa basins differs from that outside the basins. In particular, playas have higher apparent electrical conductivities than do interplaya areas at equivalent shallow depths, and lower apparent conductivities at equivalent deeper depths. This observation is con-

sistent with the dissolution-induced subsidence model of playa formation, where the deeper, less conductive material represents highly porous and possibly disturbed deposits, and the shallow, more conductive material represents lacustrine basin fill with high clay content. This model implies that the FGZ that perches groundwater may not be continuous across the playas.

Areas of elevated apparent conductivity at perched aquifer and FGZ depths around Playa 1 and in the Pantex Southeast area can be interpreted to reflect increased thickness of the FGZ and perched aquifer. Elevated apparent conductivities extend a short distance across FM 2373 in both areas, where they are replaced by lower apparent conductivities indicative of a thinner FGZ and perched aquifer. This area is characterized by high levels of cultural noise that might affect the accuracy of the conductivity data and the hydrogeological interpretations made from the data.

Major remaining tasks include integrating available geological and hydrological data from survey area wells and borings, establishing the relationship between stratigraphic and hydrologic characteristics and measured apparent conductivity, analyzing the combined information to assess the integrity and extent of the FGZ, and preparing a final report summarizing project results.

INTRODUCTION

This interim report presents preliminary results of the airborne geophysical survey flown on and near the Pantex Plant in March 2003 (fig. 1). The purpose of this survey is to measure the magnitude and variation of apparent electrical conductivity of the subsurface to help assess the extent and integrity of the middle Ogallala fine-grained zone (FGZ) that perches groundwater above the main Ogallala aquifer. This study follows the feasibility study conducted at the Pantex Plant in 2000 (Paine, 2000) that was part of the Innovative Treatment Remediation Demonstration (ITRD) program at Sandia National Laboratories. The feasibility studies were conducted in response to a recommendation in the "Protecting the Ogallala Aquifer II" report (U.S. Department of Energy, 2000) that "geophysical methods such as time domain electromagnetic soundings (TDEM) and seismic methods should be considered" to provide information on the areal extent, thickness, and lithologic variability of the perched water aquitard in the southeast plume area.

This report summarizes activities to date, which have largely focused on airborne geophysical survey data. Significant work remains before the project is complete, particularly in integrating geophysical results with stratigraphic and hydrologic data available from numerous existing wells and borings on and near the plant. Results from the completed study will be presented in a final comprehensive report before the project ends in May 2004.

FGZ Physical Properties

Numerous borings and wells have reached the FGZ during Pantex Plant operation, characterization, and remediation activities. Subsurface data indicate that the FGZ is composed of several distinct clay-rich layers within a coarser-grained matrix (Gustavson and others, 1995). Electrical logs from Pantex and surrounding wells verify the common observation that high clay content translates to increased electrical conductivity of the sediment (fig. 2). Borehole seismic measurements in an Ogallala monitoring well south of Playa 2 (BEG-PTX2) document an in-

Figure 1. Aerial photomosaic of the Pantex Plant area showing the east, north, south, and west airborne geophysical survey blocks. Aerial photographs taken in 1995 and acquired from the Texas Natural Resource Information System.

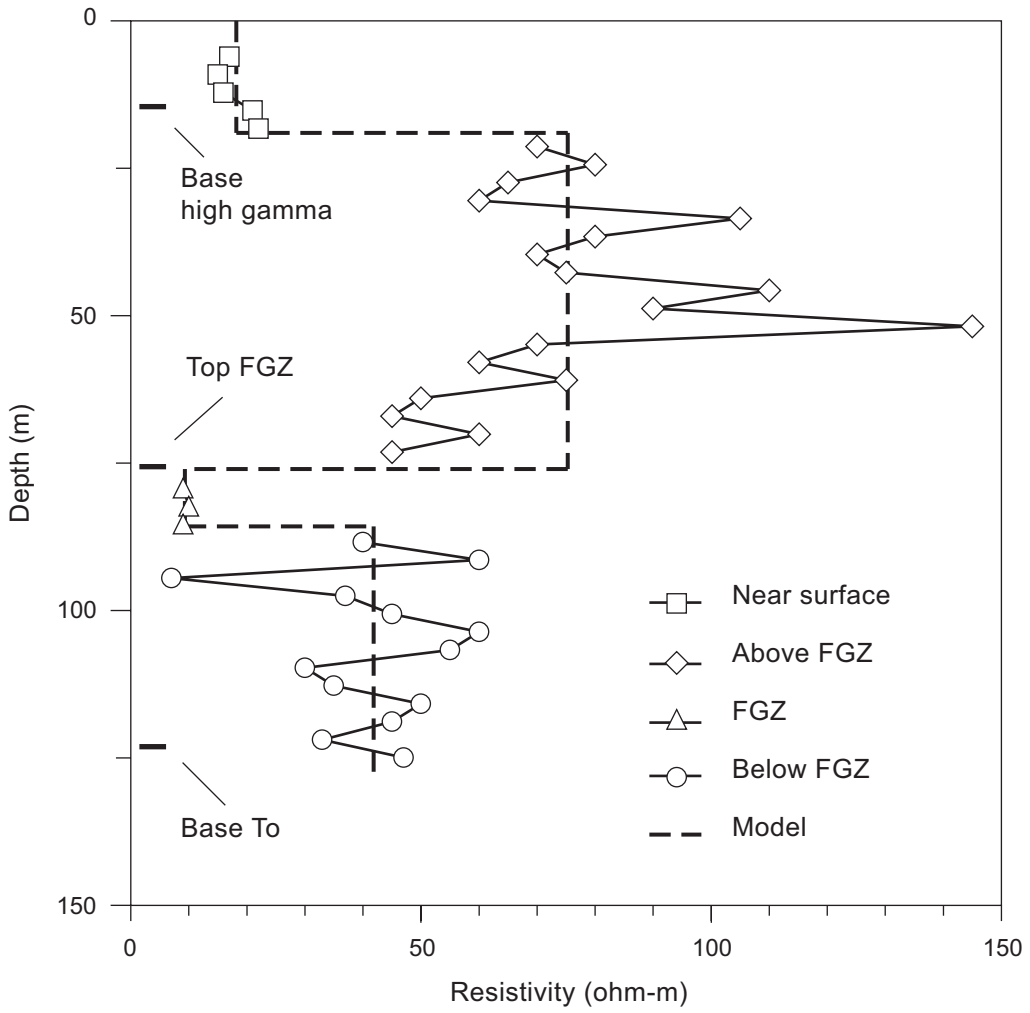

Figure 2. Resistivity log (solid line and symbols) and generalized resistivity model (dashed line) for well BEG-PTX2 in the southwest part of the Pantex Plant. Also shown are the depths to the base of the high-gamma-count zone, the top of the middle Ogallala FGZ, and the base of the Ogallala Formation (To).

crease in seismic velocity within the FGZ. Further, water-saturated sediment within the perched aquifer likely has higher density, seismic velocity, and electrical conductivity than similar unsaturated stratigraphic intervals. These observations from existing data suggest that seismic and electrical methods are appropriate tools to investigate the FGZ and associated perched aquifer. Variations in density, sediment type, and water saturation within the perched aquifer and FGZ might be large enough to image using seismic reflection methods, including the top and perhaps the base of the FGZ where it is sufficiently thick. Increases in electrical conductivity caused by water saturation within the perched aquifer and by increased clay content within the FGZ might be detected using surface or airborne electromagnetic induction methods, especially TDEM.

The design and feasibility of seismic reflection and EM surveys depend upon the depth and thickness of the FGZ and perched aquifer. Using values reported in the groundwater program management action process (Pantex Plant Environmental Restoration Department, 2000), depth to perched water averages 73 m. Saturated thickness averages 4 m, ranging from 0 to about 23 m. The underlying FGZ is reached at an average depth of 78 m. Its thickness is poorly constrained, but existing data suggest an average thickness of about 16 m. Consequently, the depth range of interest ranges from about 60 to 120 m; the combined thickness (FGZ and saturated zone) averages about 20 m.

Preliminary Modeling and Ground-Based TDEM

We tested the feasibility of the TDEM method in addressing issues related to the perched aquifer at the Pantex Plant by performing preliminary modeling and reconnaissance field investigations in the Pantex Southeast and Playa 3 areas (Paine, 2000). Because electrical properties change with changes in clay content and water saturation, methods that measure subsurface electrical conductivity show promise in detecting subsurface changes caused by the presence or absence of the FGZ and variations in the thickness of the FGZ and the saturated thickness of the perched aquifer.

The purpose of TDEM modeling was to determine (a) appropriate acquisition parameters for the field survey and (b) whether anticipated changes in thickness of the FGZ would produce detectable differences in the TDEM data. Little information has been collected to date on the electrical properties of strata beneath the Pantex Plant; available data consists of complete induction logs for wells BEG-PTX2 and BEG-PTX3, a few partial induction logs in the Pantex Southeast and Playa 3 areas covering only the well depths below the FGZ, and resistivity logs from public water-supply wells north of the Pantex Plant.

We produced a generalized series of subsurface resistivity models based on resistivity data from well BEG-PTX2, located southwest of Zone 11 and south of Playa 2 (fig. 1). Logs of this and other wells show that resistivity changes within the Blackwater Draw and Ogallala formations can be generalized into four layers (fig. 2). These layers are, from shallowest to deepest: (1) a low-resistivity (about 20 ohm-m) layer a few tens of meters thick having high gamma counts and relatively high clay content that roughly corresponds to the Blackwater Draw Formation; (2) an upper Ogallala resistive layer averaging about 75 ohm-m that extends to a depth of about 75 m at BEG-PTX2; (3) a low-resistivity layer of about 9 ohm-m that is about 10-m thick, representing the middle Ogallala FGZ; and a lower Ogallala resistive layer averaging about 45 ohm-m that extends to the base of the Ogallala Formation. Geophysical logs that penetrate pre-Ogallala rocks suggest that the basal Ogallala layer is underlain by a low-resistivity unit, but that unit was not logged in well BEG-PTX2.

To simulate the effect of varying FGZ thicknesses on the TDEM data, we computed and compared the TDEM measurements that would be expected using the resistivities and layer thicknesses of the generalized model, varying the thickness of the FGZ from 0 to 10 m in 1-m increments. Predicted strength of the transient signal differs significantly at times later than about 0.5 milliseconds (ms) after shutoff of the transmitter current for the two end-member models of no FGZ and a 10-m thick FGZ (fig. 3). When the signal strength data are converted to apparent resistivity (fig. 4), the greatest divergence in the curves occurs between about 0.2 and 5 ms after current termination. If the only stratigraphic variable is the FGZ thickness, modeling data suggest

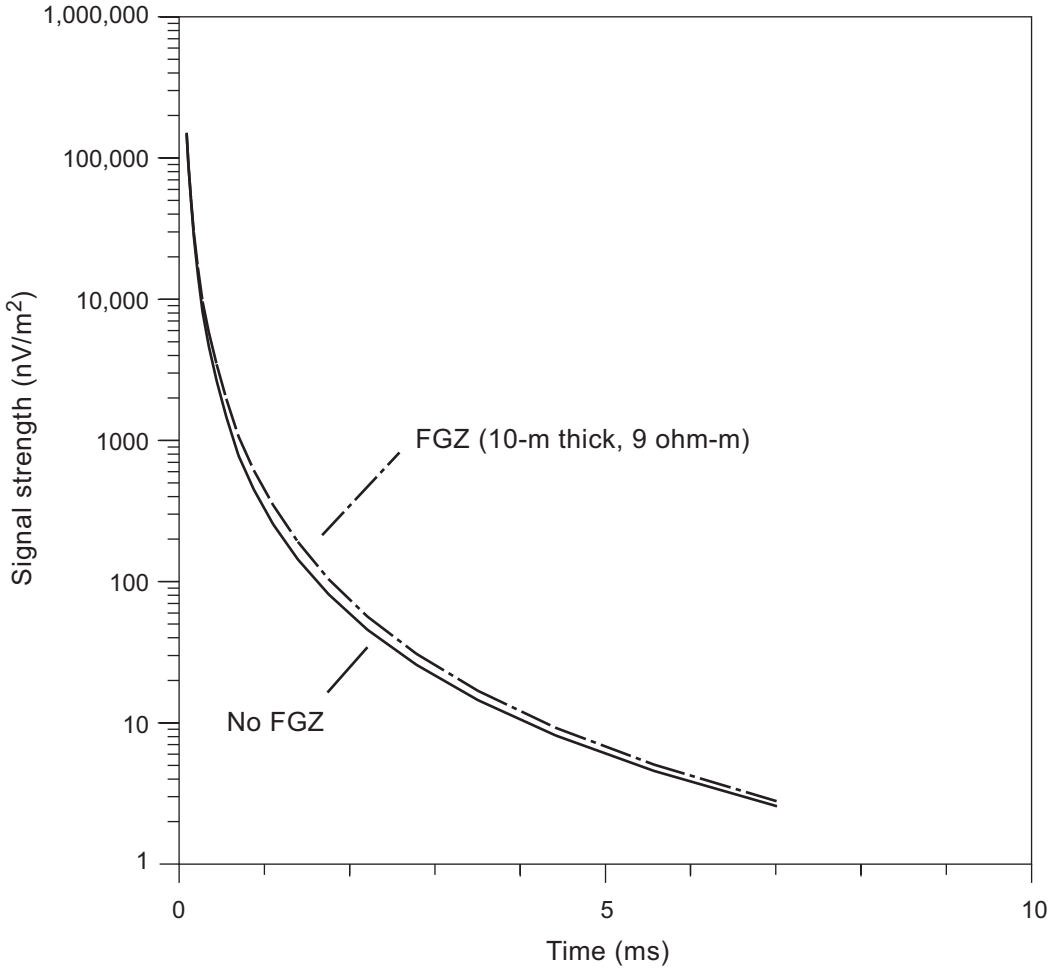

Figure 3. Predicted transient signal for the generalized resistivity model from well BEG-PTX2 with (solid line) and without (dashed line) a 10-m-thick FGZ having 9 ohm-m resistivity.

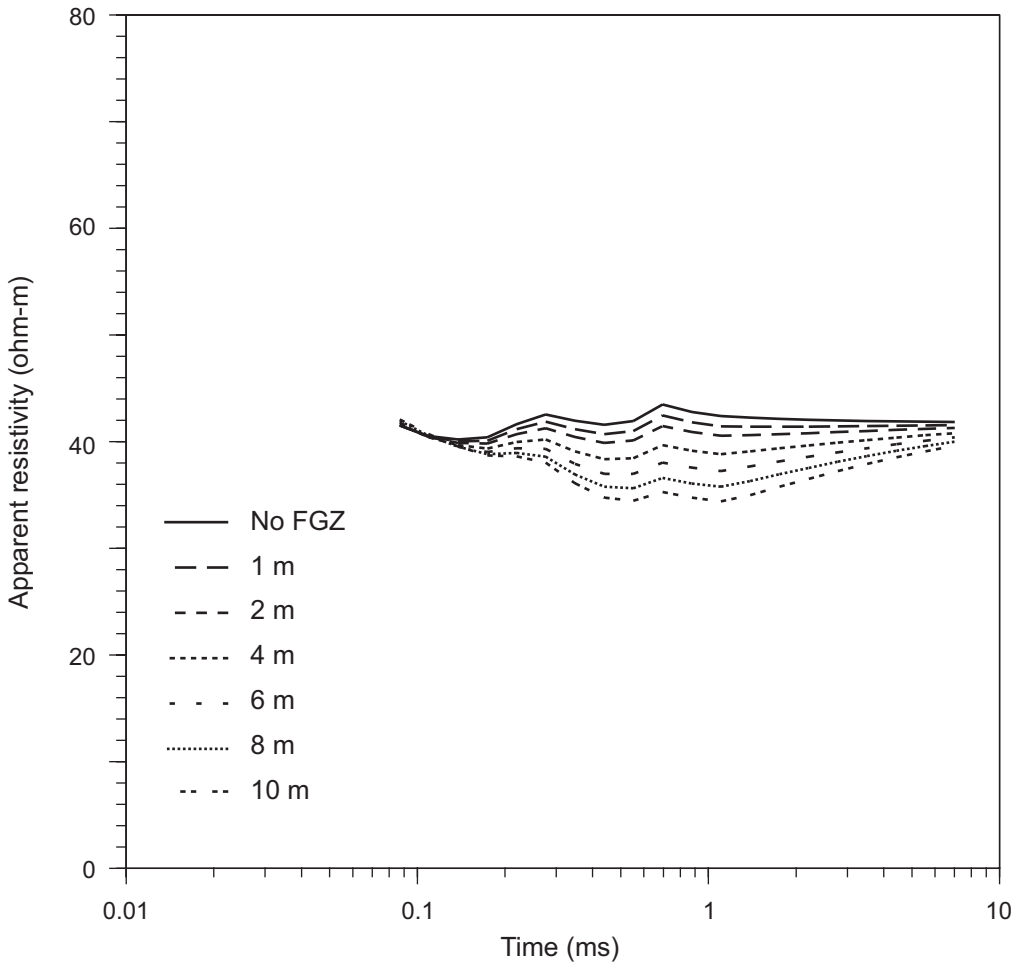

Figure 4. Predicted apparent resistivity curves for the generalized resistivity model from well BEG-PTX2 assuming FGZ thicknesses ranging from 0 (FGZ absent) to 10 m.

that small changes in FGZ thickness are detectable and that field data should be recorded between about 0.1 and 10 ms after current termination to best detect FGZ thickness changes.

We acquired ground-based TDEM soundings in the Playa 3 and Pantex Southeast areas (fig. 5) to evaluate the method for detecting changes in Ogallala stratigraphic and hydrological properties and to determine electrical properties of the ground for airborne survey design (Paine, 2000).

Transient signals recorded for each sounding show similar trends. According to modeling results, these signals are sufficiently long to contain information about subsurface electrical properties to depths beyond those of the FGZ. Changes in slope of each decay curve result from changes in electrical properties encountered as the primary signal travels deeper into the subsurface. Variability in decay shapes among transients indicates that the subsurface resistivity profile differs from site to site.

At each sounding location, we constructed resistivity models of the subsurface, calculated the transient for those models, compared the calculated transients to the actual transient, and adjusted the model iteratively until it provided an adequate fit to the observed data. Two- to four-layer models constructed for soundings along the south–north series in the Pantex Southeast area differ relatively little in the near-surface low resistivity layer (fig. 6), but differ more at deeper levels. Within what would correspond to the upper Ogallala resistive zone and the middle Ogallala FGZ, resistivities decrease progressively to the north. Highest resistivities at the FGZ depth are calculated for sounding TDEM 1 at the south end of the series; lowest resistivities are calculated for TDEM 10 near the Pantex east gate. Maps of FGZ thickness derived from Ebasco seismic data (U. S. Army Corps of Engineers, 1992) show the FGZ thickness progressively increasing northward along this series, matching the TDEM trend. The FGZ does not appear in the model as a discrete, resolvable layer, but appears to be a major influence on resistivity calculated for the resistive intermediate layer. Decreases in resistivity to near 10 ohm-m in the model layers corresponding to the lower part of the Ogallala occur near the depth reported for the

Figure 5. Reconnaissance ground-based TDEM sounding sites (appendix A).

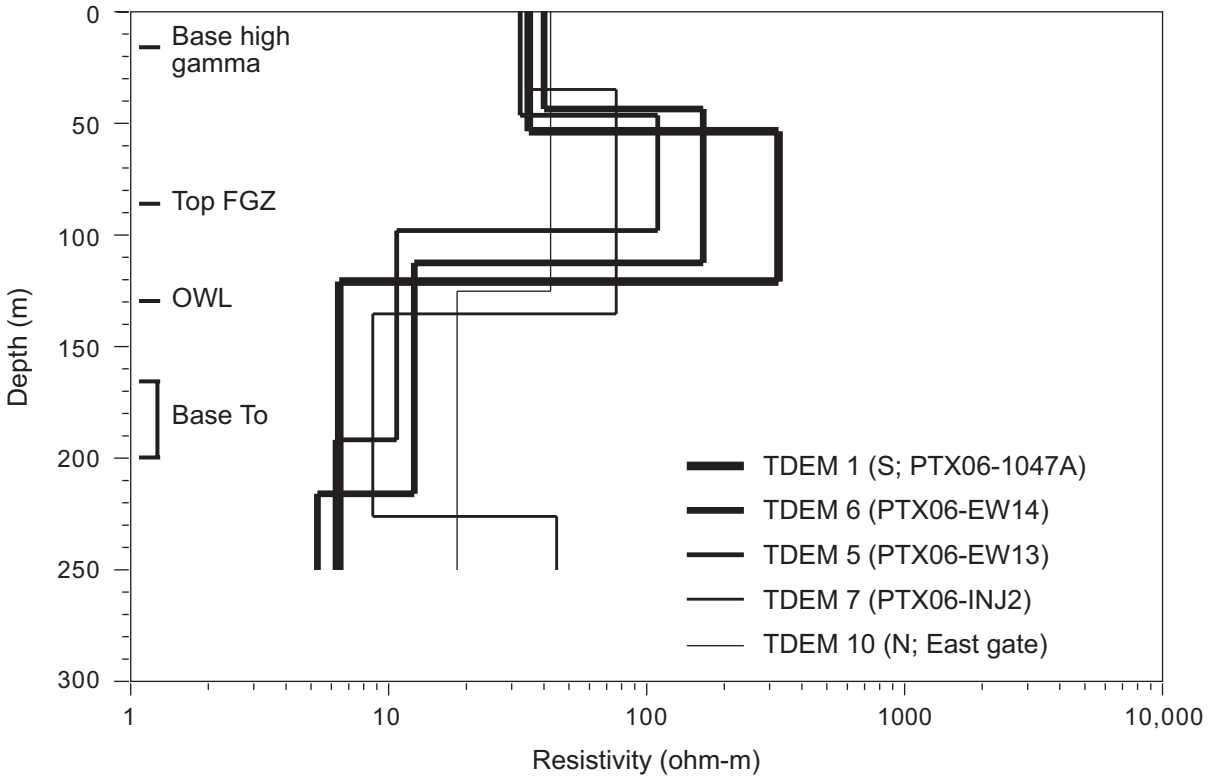

Figure 6. Two- to four-layer resistivity models that fit transients recorded at sites TDEM 1, 5, 6, 7, and 10 in the Pantex Southeast area. Also shown are the approximate depths to the base of the high-gamma-count zone, the top of the middle Ogallala FGZ, the Ogallala water level (OWL), and the base of the Ogallala Formation (To).

Ogallala water level. Further resistivity changes at deeper depths in the models are at or deeper than the reported base of the Ogallala.

Rationale for an Airborne TDEM Survey

Modeling studies and 10 ground-based TDEM soundings showed that the thickness of the FGZ can influence the strength and shape of the TDEM signal, suggesting that TDEM could be used to help evaluate the extent and integrity of the FGZ. Airborne TDEM instruments offer the ability to obtain spatially dense data required to identify expected subtle stratigraphic and hydrologic changes associated with the FGZ. These instruments are flown at low altitude along closely spaced flight lines, enabling thousands of soundings to be acquired in the same time required to collect a few ground-based soundings. Based on the results of modeling and ground-based TDEM soundings and in consultation with Pantex Plant staff, we designed and conducted an airborne geophysical survey of four areas north, east, south, and west of the Pantex Plant (fig. 1).

METHODS

We employed airborne geophysical methods to rapidly and noninvasively measure changes in electrical conductivity with depth in the four survey blocks surrounding the Pantex Plant (fig. 1). The principal geophysical method is electromagnetic induction, or EM (Parasnis, 1973; Frischknecht and others, 1991; West and Macnae, 1991). This family of geophysical methods employs a changing primary magnetic field that is created around a current-carrying transmitter wire to induce a current to flow within the ground, which in turn creates a secondary magnetic field that is sensed by a receiver coil. In general, the strength of the secondary field is proportional to the conductivity of the ground.

TDEM methods (Kaufman and Keller, 1983; Spies and Frischknecht, 1991) measure the decay of a transient, secondary magnetic field produced by the termination of an alternating primary electric current in the transmitter loop (fig. 7). The secondary field, generated by current

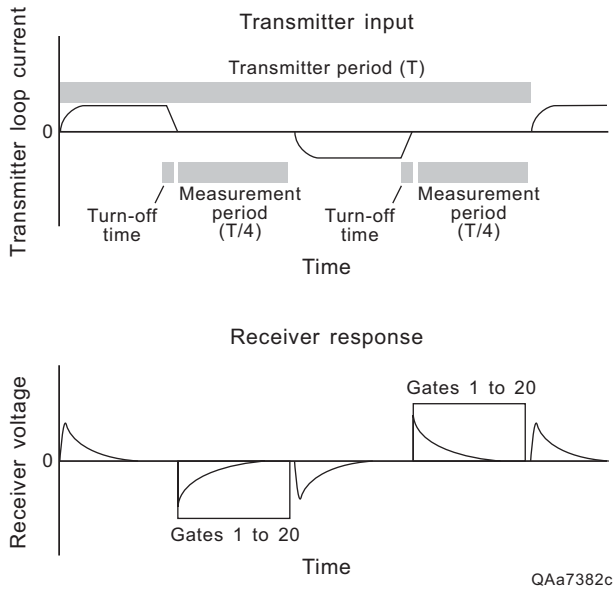

Figure 7. TDEM transmitter input (upper graphic) and receiver response (lower graphic). Adapted from Geonics Limited (1992).

induced to flow in the ground, is measured by the receiving coil following transmitter current shutoff. Secondary field, or transient, strength at an early time gives information on conductivity in the shallow subsurface; transient strength at later times is influenced by conductivity at depth.

Airborne geophysical data, including TDEM and magnetic-field data, were acquired over the Pantex survey blocks in March 2003 by Fugro Airborne Surveys (table 1). The combined 120-km^2 area was covered by flying north–south lines spaced at 100 m in the east and west blocks and east–west lines spaced at 100 m in the north and south blocks (fig. 8). A total of 104,880 measurement locations were acquired over the survey flight distance of 1,243 km. Fugro collected EM and magnetic-field data using its GEOTEM 1000 TDEM system and a cesium magnetometer towed behind a Casa 212 twin-engine aircraft (fig. 9). Flight height was 120 m; the three-axis EM receiver was towed 130 m behind the transmitter at a height of 70 m above the ground (table 2). The primary EM field was generated by a six-turn wire loop fixed to the aircraft carrying a 30-Hz, discontinuous sinusoidal current of 560 amperes (A). The dipole moment, a measure of transmitter strength, was 776 x 10^3 A-m^2, more than an order of magnitude larger than the moment calculated for the ground-based instrument used in the feasibility study. Transients were recorded during the 11.3-ms window following termination of the 4-ms transmitter pulse. EM diffusion depth, the depth below which currents will not have diffused during the measurement period, is commonly used as a proxy for exploration depth. It is calculated using the equation

$$d = k (t \ r)^{0.5}$$

where d = diffusion depth (in m), k = 503.3 (m/ohm-s)$^{0.5}$, t = latest time measured, and r = resistivity (in ohm-m) (Parasnis, 1986).

Assuming a ground conductivity of 20 to 50 mS/m (50 to 20 ohm-m resistivity) estimated from ground-based TDEM data and a latest measurement time of 11.3 ms, expected exploration depth is about 240 m for the most conductive ground and about 380 m for the least conductive ground. Measurement locations were determined from global-positioning-system (GPS) data by using a base station at the Amarillo airport and a roving receiver on the aircraft. Locational

Table 1. Flight specifications for the Pantex airborne geophysical survey conducted in March 2003.

Company	Fugro Airborne Surveys, Ottawa, Ontario, Canada
Acquisition date	March 8–13, 2003
Aircraft	Casa 212 (twin engine)
Flight line spacing	100 m
Flight line direction	North–south (east and west blocks); east–west (north and south blocks)
Flight height	120 m
Altimeter	Radar; 0.3 m sensitivity; sample frequency 1 Hz
Navigation	Differential GPS (~5 m accuracy); sample frequency 1 Hz
Flight speed	125 knots; 145 mi/hr; 232 km/hr; 65 m/s
Distance surveyed	1,243 km
Area surveyed	120 km^2
Measurement locations	104,880

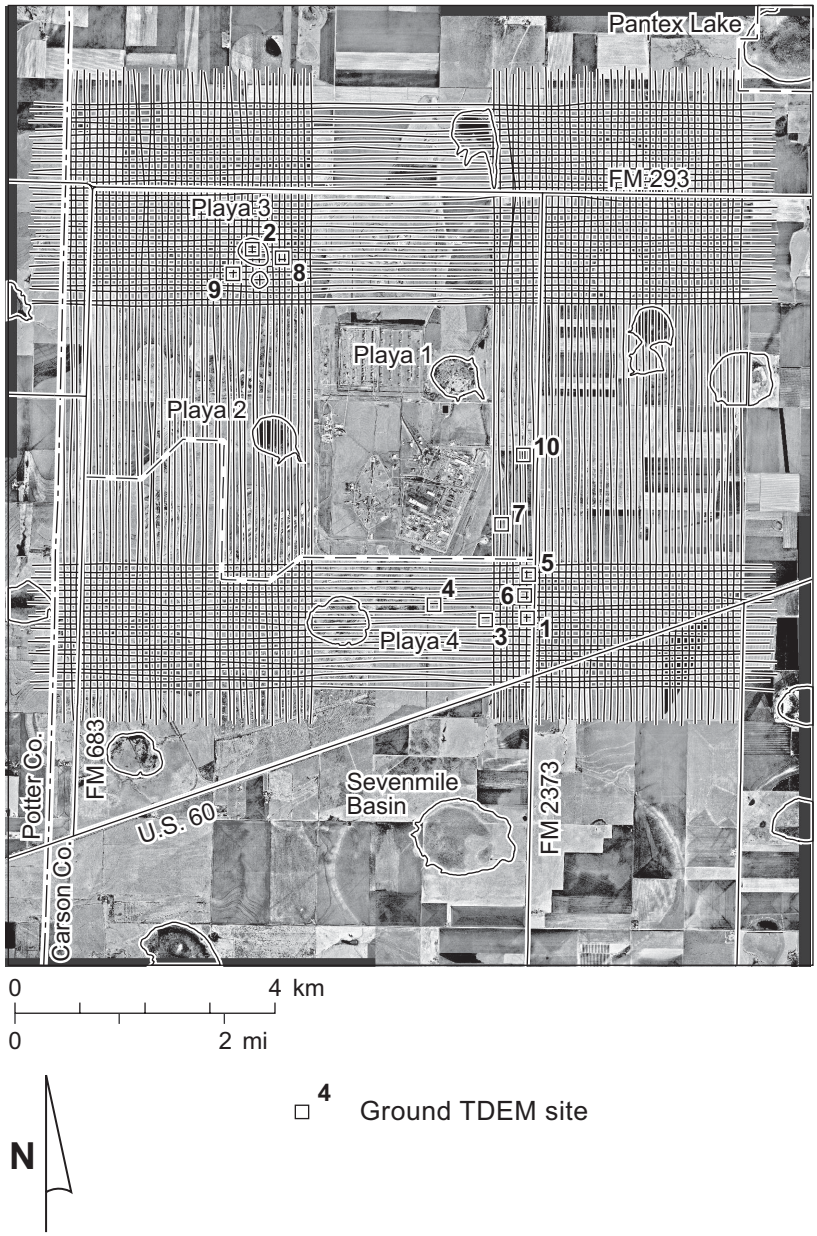

Figure 8. Map of the Pantex Plant area showing geophysical survey flight lines in the north, east, south, and west blocks. Also shown are ground TDEM locations.

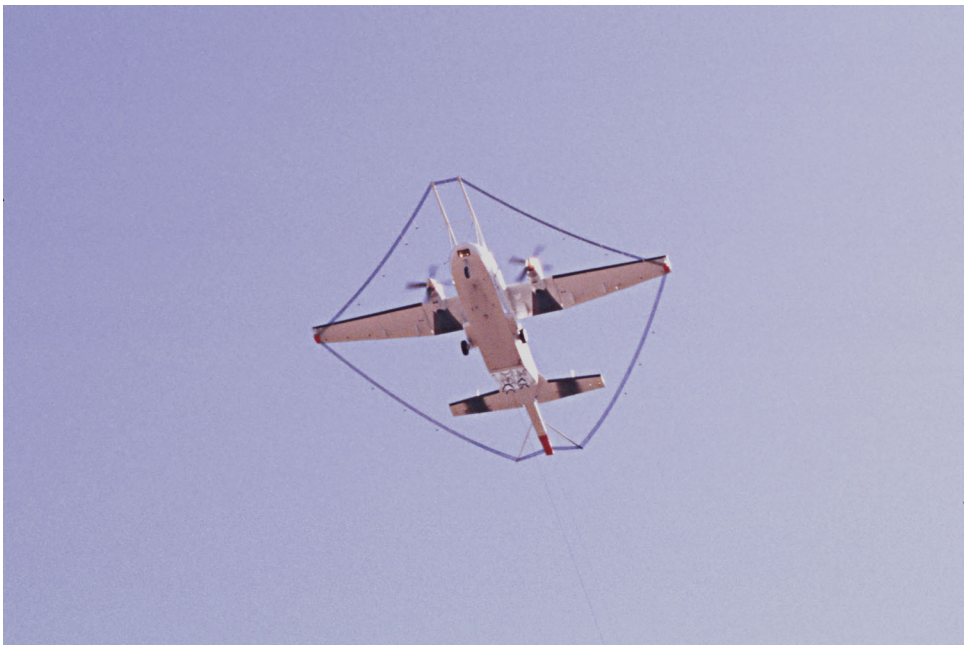

Figure 9. Casa 212 aircraft acquiring TDEM and magnetic field data in the Pantex area. The TDEM transmitter is looped around the aircraft, which is towing the TDEM receiver and magnetometer (not shown).

Table 2. GEOTEM system acquisition parameters used for the Pantex airborne electromagnetic induction survey conducted by Fugro Airborne Surveys, March 2003.

EM system	GEOTEM 1000
Transmitter loop area	231 m^2
Number of transmitter loops	6
Transmitter loop current	560 A
Transmitter dipole moment	~776,000 A-m^2
Transmitter frequency	30 Hz
Transmitter on time	4.1 milliseconds
Transmitter height	120 m
Receiver type	Towed 3 axis
Receiver height	70 m
Receiver trailing distance	130 m
Number of recording windows	20
Time span of recording window (from end of pulse)	-3.9 to 11.3 ms
Sample rate	4 Hz
Sample interval	~16 m

accuracy is 5 m or better. At the 30-Hz transmitter frequency (60-Hz sample frequency) and a nominal airspeed of 232 km/hr, transients were acquired every 1.1 m along the flight line. Recording stacked transients at 4 Hz resulted in a sample spacing of about 16 m. Fugro processed and delivered the data in March 2003 (Fugro Airborne Surveys, 2003).

Along with the transients measured in the *x* (parallel to the flight path), *y* (horizontal and perpendicular to the flight path), and *z* (vertical) axes by the towed receiver coils, Fugro performed conductivity-depth transforms to produce relatively smooth conductivity models depicting a conductivity value at 10-m-depth intervals. These transforms were performed for all 104,880 stacked transients.

We produced horizontal images of subsurface conductivity for each survey area by (1) extracting modeled conductivity values at 10-m-depth intervals; (2) gridding the values within the image processing software ERMapper using a cell size of 20 m; (3) manually rescaling the color bar for each depth slice to match the apparent conductivity range, and (4) exporting the georeferenced images using the Universal Transverse Mercator (UTM) zone 14 north projection and the 1983 North American Datum.

Digital images were imported into a GIS database. Coverages being used to analyze the relationship between the geophysical data and geological and hydrological characteristics of the area include borings, water wells, water-quality analyses, aerial photographs, and roads (and associated power lines).

The aircraft also towed a cesium magnetometer at a height of 73 m above the ground (table 3) to measure changes in the magnetic field strength caused by natural effects and local features such as pipelines that contain significant amounts of iron. Magnetometer data were acquired at 10 Hz, yielding a 7-m sample spacing for magnetic field data.

Table 3. Acquisition parameters used for the Pantex airborne magnetometer survey conducted by Fugro Airborne Surveys, March 2003.

Magnetometer	Towed cesium vapor (Scintrex Cs-2)
Magnetometer height	73 m
Sample rate	10 Hz
Sample interval	~7 m
Sensitivity	0.01 nT; 0.2 ppm

AIRBORNE GEOPHYSICAL SURVEY RESULTS

Fugro Airborne Surveys processed the airborne geophysical data and delivered digital survey products in March 2003 that included surface topography, magnetic field strength, and several types of TDEM data. Among the types of data relevant to the TDEM measurements were powerline noise, two types of secondary signal strength, apparent ground conductivity, and transforms of the TDEM signal to pseudo conductivity profiles (conductivity-depth transforms, or CDTs) at each measurement point.

Terrain, Magnetic Field Strength, and Powerline Noise

Aircraft height above the ground is one of the important parameters used in determining the electrical properties of the ground in response to an airborne instrument. GPS instruments on the aircraft and at the base station allow accurate positioning of the aircraft during the survey, but the surface topography is typically not well known. Data from an onboard altimeter can be combined with GPS data on aircraft position to produce a terrain map of the ground surface (fig. 10). This map shows obvious and subtle topographic features that include a general decrease in surface elevation from northwest to southeast and prominent topographic lows associated with each of the playas and surrounding basins. Surface elevation ranges from 1057 to 1098 m above sea level. Minor errors in aircraft position appear as linear lows or highs along the flight line direction (figs. 8 and 10).

Magnetic field data were not a principal objective, but can be helpful in identifying pipelines, wells, and other significant structures that might affect the TDEM signal. Only the total magnetic field strength is measured by the towed magnetometer, but local magnetic anomalies can be enhanced by creating a residual magnetic anomaly map (fig. 11) by calculating the difference between the measured field strength and the field strength predicted from a global data base of magnetic field strength values (the International Geomagnetic Reference Field, or IGRF). In addition to the dominant, northwest-trending U-shaped feature that reflects deeper geologic

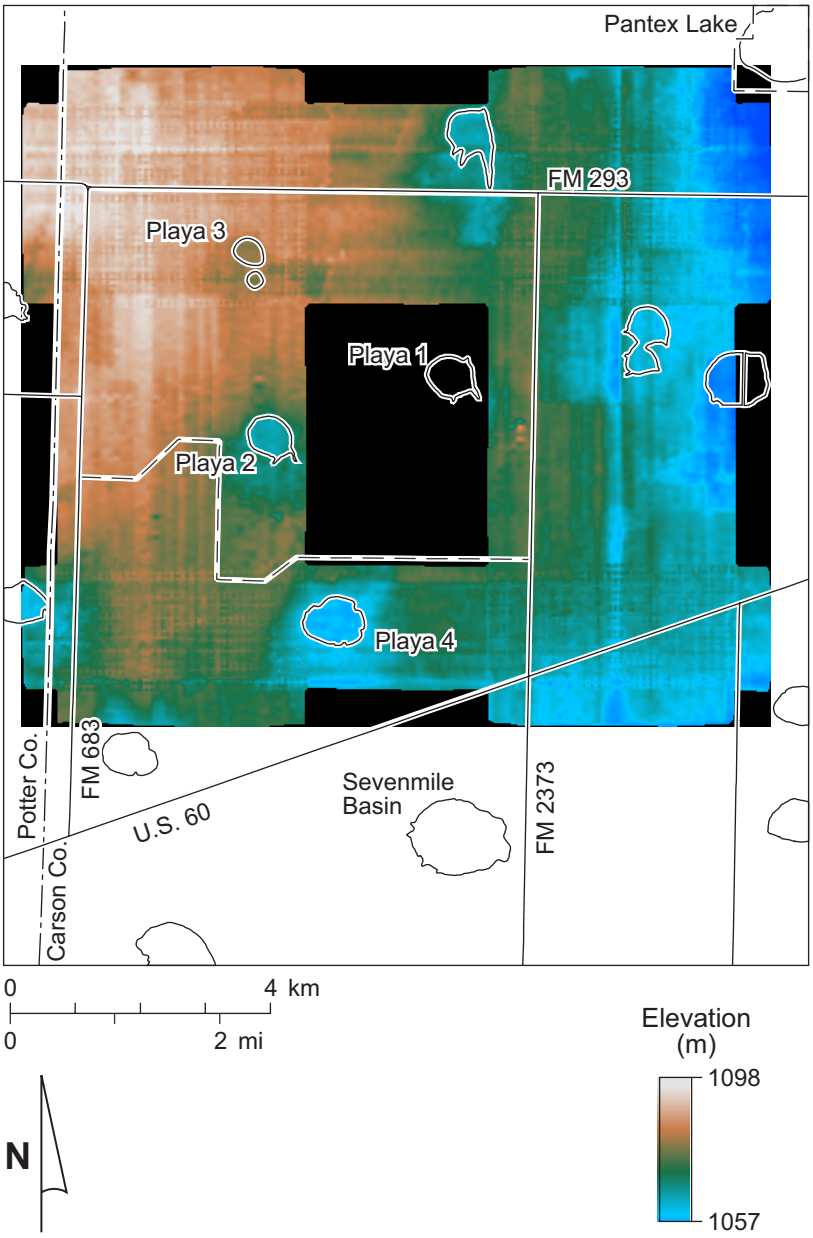

Figure 10. Terrain map of the Pantex Plant area derived from aircraft position and altimeter data.

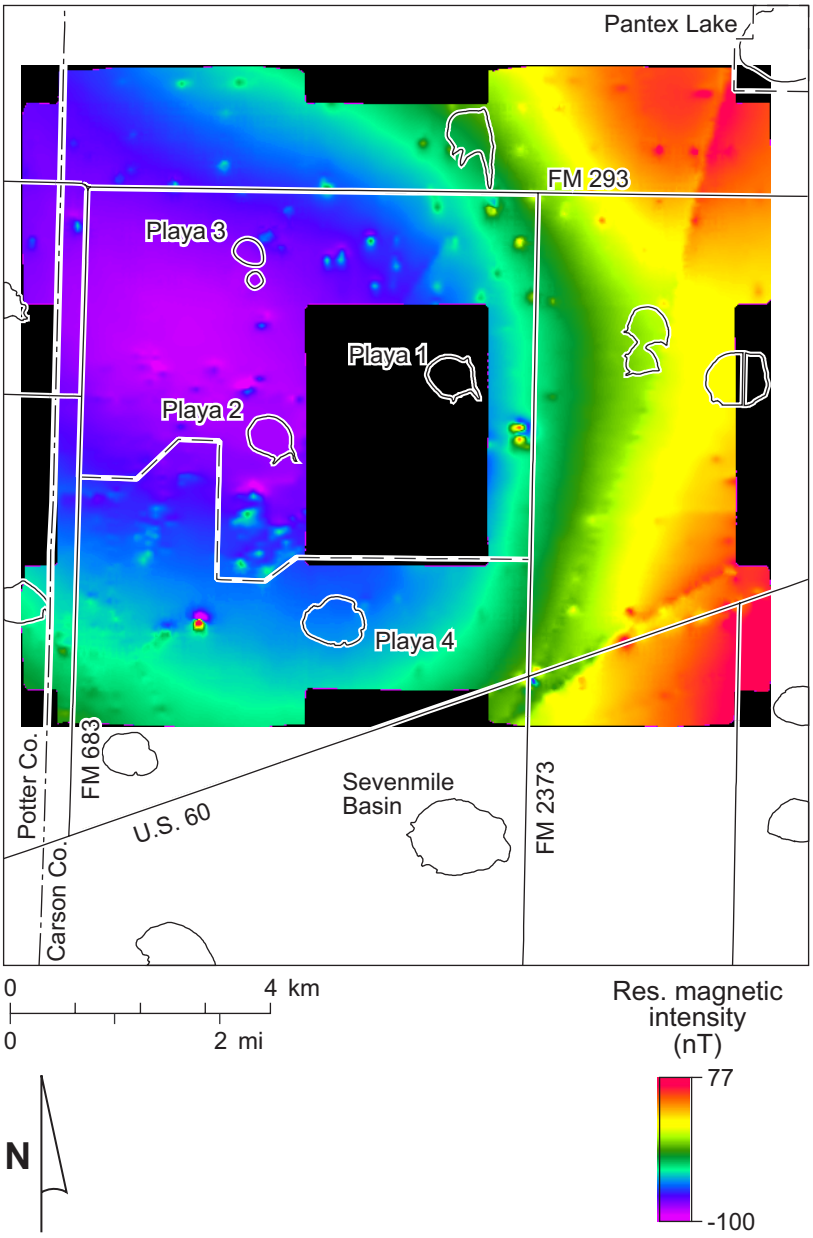

Figure 11. Residual magnetic field strength map of the Pantex Plant area. Positive values are areas where measured field strength is higher than reference field (IGRF) values; negative values are areas where measured field strength is lower than IGRF values.

structure, many local anomalies are evident that coincide with known wells and structures. Two prominent linear features that trend north-northeast and east-northeast on the east side of the survey area are typical pipeline signatures. Total magnetic field strength ranged from 51,544 to 51,693 nanoteslas (nT) over the combined survey area.

Electric power lines carry alternating current that produces magnetic fields. These fields are strong enough to interfere with the relatively weak secondary electrical signals generated in the ground by the airborne TDEM transmitter. We used data from an onboard powerline noise monitor to create a map depicting noise levels across the survey area (fig. 12), then used those values to identify excessively noise-contaminated areas in the TDEM data set. Powerline noise varied greatly in strength across the area, ranging from values at or below 1 millivolt (mV) to as high as 500 mV. Highest values are observed on flight lines where the aircraft crosses major power lines. On these lines, the low-flying receiver passes closer to the power lines than it does when the flight lines are parallel to the same power lines. We used a threshold powerline noise value of 15 mV to remove excessively noisy data from the TDEM data set. Airborne TDEM soundings with powerline noise less 15 mV were used to generate images of apparent conductivity and conductivity-depth slices.

TDEM Signal Strength and Noise Correlation

Calculations of apparent ground conductivity and changes in apparent conductivity with depth are based on the strength and decay of the TDEM signal recorded by the three-component receiver. The signals and mathematical manipulations of them are critical to the success of the TDEM method in assessing the extent and integrity of the FGZ. Fugro delivered processed TDEM data that included both the measured dB/dt signal (changes in the generated magnetic field strength over time) and its calculated integral, the B-field (magnetic field strength generated by the TDEM transmitter and ground response) (Smith and Annan, 2000). We examined these signals to evaluate the effects of powerline noise on the airborne TDEM data.

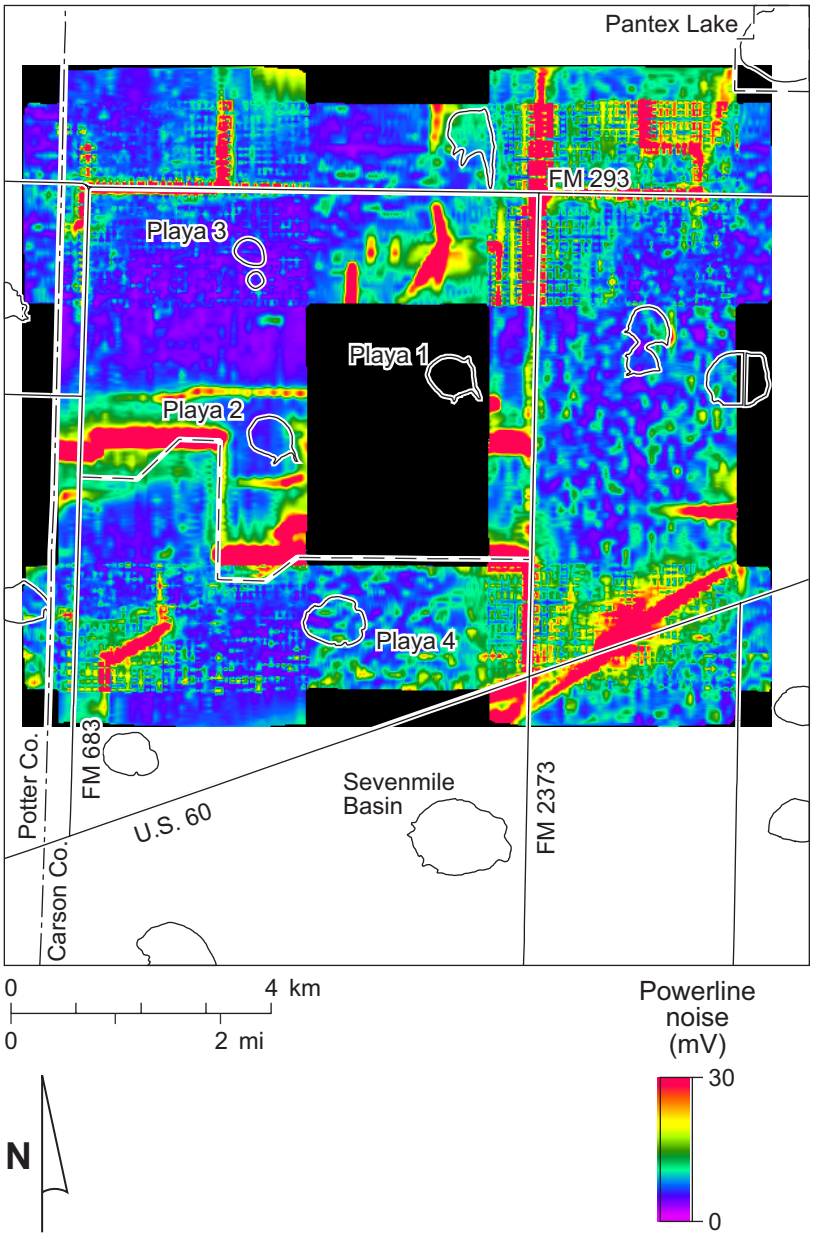

Figure 12. Powerline noise intensity map of the Pantex Plant area measured during the airborne geophysical survey.

B-field data (fig. 13) are presented in the magnetic field unit picotesla (pT, or 0.001 nT) for a single transmitter cycle. While the TDEM transmitter is on (on time, fig. 13a), there are large changes in the signal magnitude and polarity, peaking at about 1000 pT (1 nT) just before the transmitter is turned off. Once the transmitter is turned off (off time, fig. 13a), there is a rapid decay in the secondary signal generated by currents flowing in the ground (figs. 13a and b). The strongest component is in the *z* direction (vertical), followed in strength by the *x* component (in the flight-line direction). The weakest signal is recorded in the *y* direction, transverse to the flight-line direction. Above horizontally stratified layers, the *y* component should be small because the transmitter generates the strongest signal in the *z* direction (the transmitter is a vertical dipole). A large *y* signal would suggest significant lateral changes in conductivity, which might invalidate processing assumptions that are made in determining apparent conductivity of the ground and its variation with depth. The *x* component should also be stronger than the *y* component because the receiver is recording an *x* signal by moving through a magnetic field as the aircraft acquires data.

We examined the influence of powerline noise on all components of the B-field signal by calculating a correlation coefficient between powerline noise and signal strength during both on and off times (fig. 13c). The strongest correlation with noise is evident for the *x* component at relatively early off times, reaching nearly 0.5 at times of 0.5 to 1.5 ms after turnoff. Both *z* and *y* components correlate poorly with powerline noise. These data suggest that including *x*-axis data in conductivity calculations might increase the influence of unwanted noise.

The actual measured signal, dB/dt, is equivalent to the time derivative of the B-field signal and is given in units of nT/s (fig. 14). While the transmitter is on, the dB/dt signal also shows polarity and large magnitude changes (fig. 14a). Once the transmitter is off, the secondary signal arising from ground currents decays rapidly in all three components (fig. 14a and b). The *z* component is again the strongest, decaying rapidly from initial values of more than 1000 nT/s to final values above 1 nT/s. The *x*-component signal is significantly weaker than the *z* component, but is an order of magnitude stronger than the transverse, or *y*, component. Both the *z* and *y*

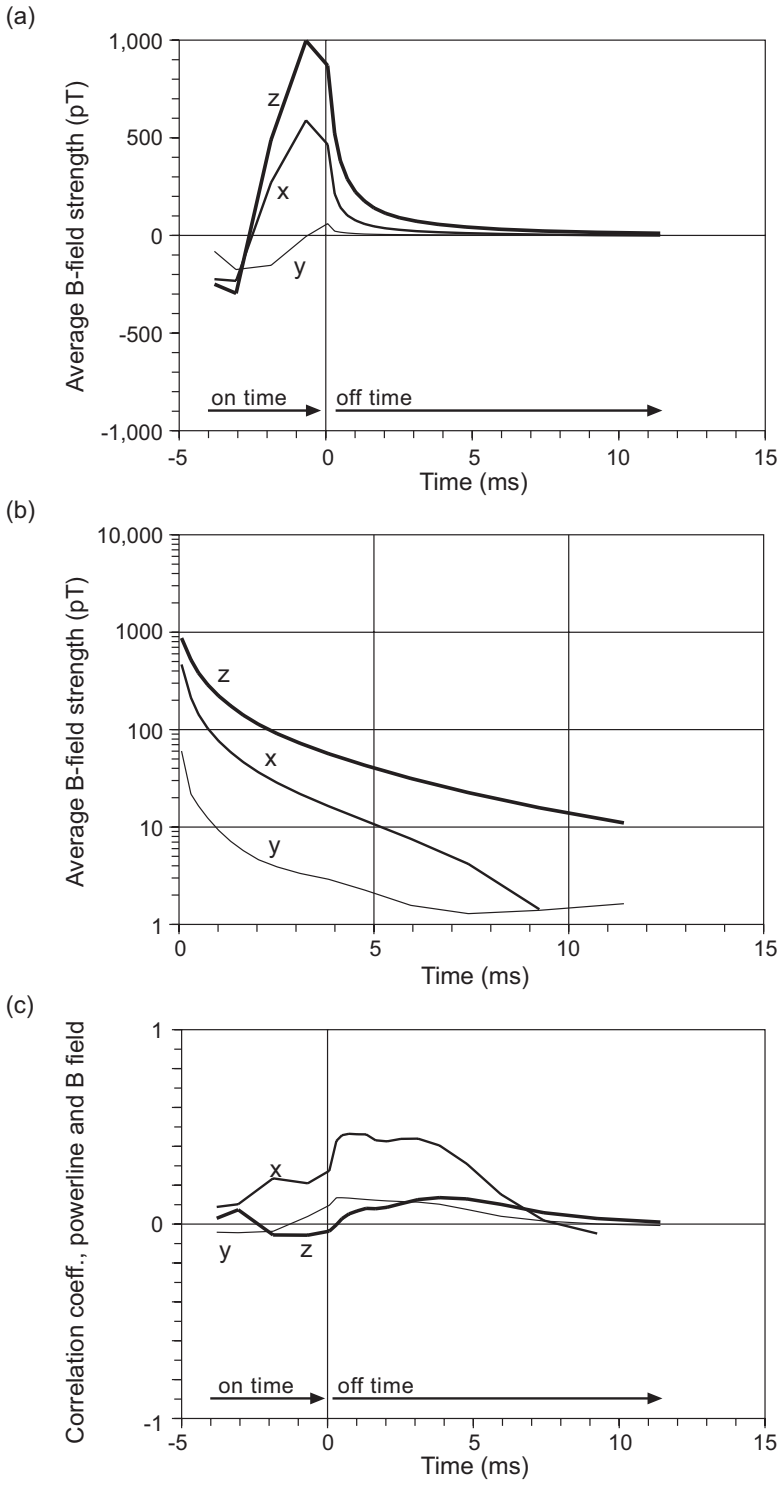

Figure 13. B-field signal strength and correlation with powerline noise. (a) B field signal strength over one TDEM transmit and receive cycle in the *z* (vertical), *x* (inline), and *y* (transverse) directions, including both on time (TDEM transmitter on) and off time (transmitter off); (b) decay of secondary TDEM B-field signal during off time in the *z*, *x*, and *y* directions; and (c) correlation of B field signal components with powerline noise during both on and off times.

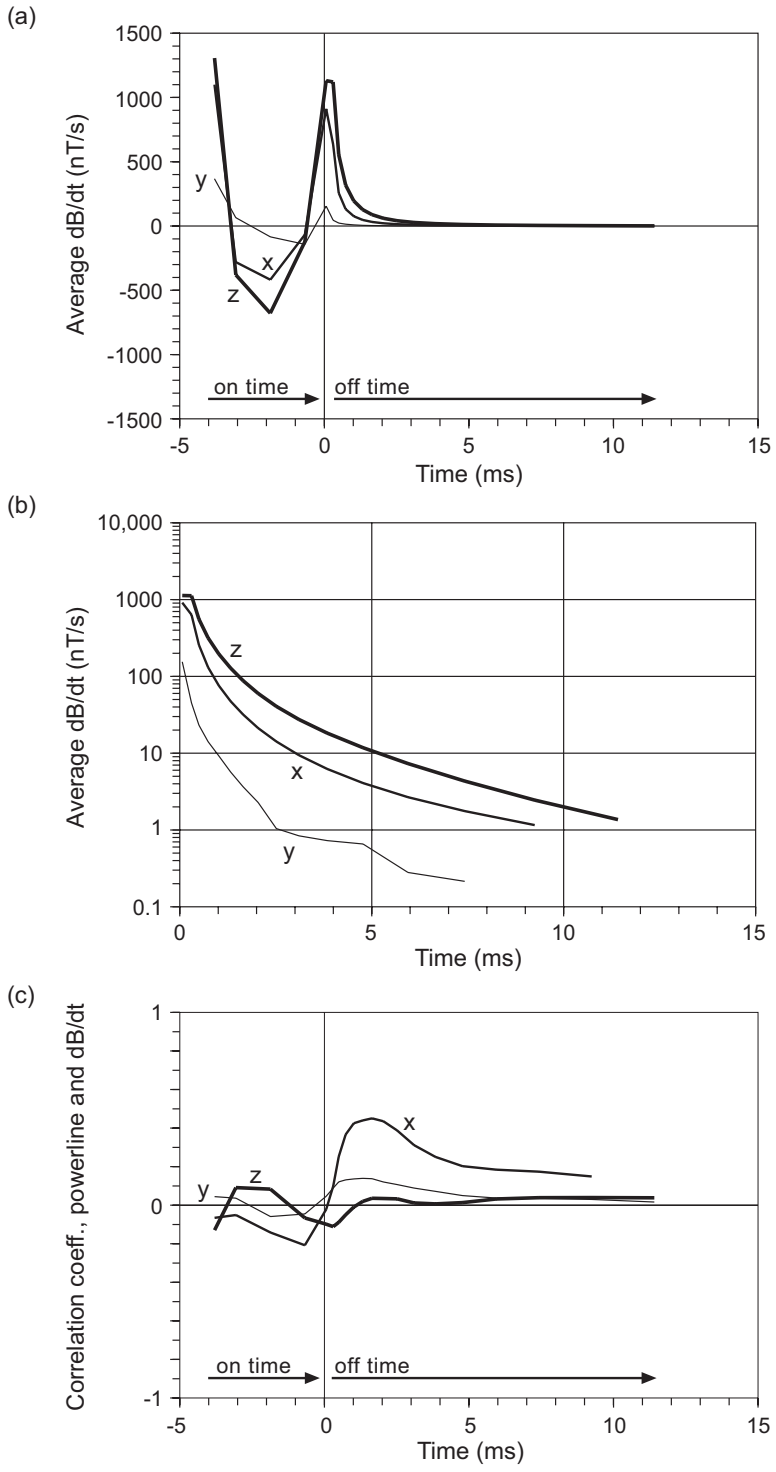

Figure 14. Time derivative (dB/dt) signal strength and correlation with powerline noise. (a) dB/dt signal strength over one TDEM transmit and receive cycle in the *z* (vertical), *x* (inline), and *y* (transverse) directions, including both on time (TDEM transmitter on) and off time (transmitter off); (b) decay of secondary TDEM dB/dt signal during off time in the *z*, *x*, and *y* directions; and (c) correlation of dB/dt field signal components with powerline noise during both on and off times.

components are poorly correlated with powerline noise (fig. 14c), but the *x* component shows a relatively high and positive correlation of about 0.5 with powerline noise, particularly at early off times.

Apparent Ground Conductivity

Rather than produce maps depicting TDEM signal strength at various times during signal decay, the TDEM signals can be processed to generate apparent conductivity models of the ground that would produce the observed signal decay. The simplest of these is a single value of apparent conductivity that best fits the observed decay at a sounding location assuming that the ground beneath the instrument is electrically homogeneous. This image (fig. 15), with noisy soundings removed, can be used to observe general trends. Calculated apparent conductivities for the combined survey blocks range from 38 to 102 mS/m. Relatively high values are present at each of the on- and off-plant playas, over a large area north of FM 293 (both west and east of the Pratt playa), and within areas extending east and southeast of the Pantex Plant. Relatively conductive areas such as these suggest higher clay and water content within the exploration depth of the instrument.

Conductivity-Depth Transforms (CDTs)

Single apparent conductivity values for each sounding location are useful for establishing basic electrical properties of an area and identifying major trends, but are an oversimplification of the ground's electrical properties at Pantex that are known to vary significantly as sediment type and water saturation change with depth (fig. 2). During TDEM processing, Fugro also produced "transforms" depicting changes in apparent conductivity with depth (CDTs) at each sounding location. These are not full, robust inversions of the TDEM data (Wolfgram and Karlik, 1995), but do produce pseudo-depth profiles from z and x axis data that reflect changes in signal strength with time.

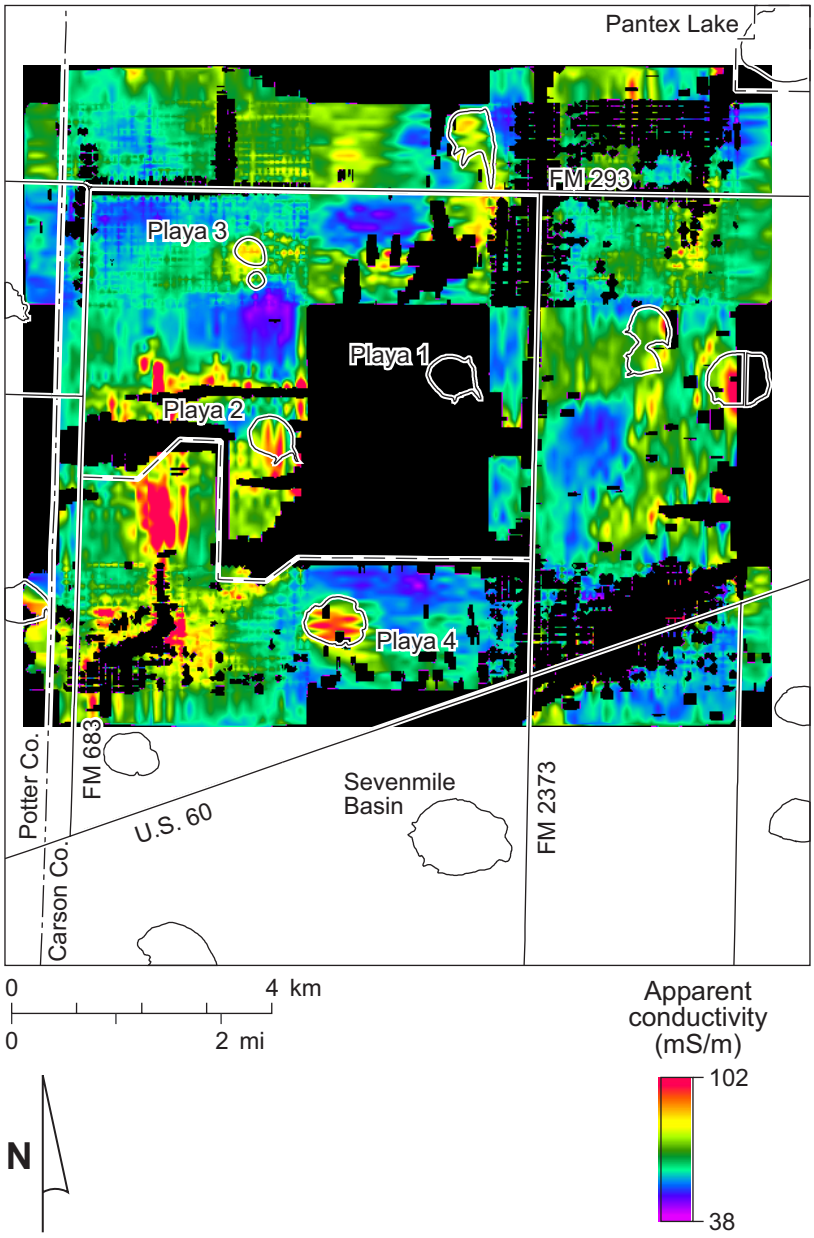

Figure 15. Apparent conductivity map of the Pantex Plant area with data from noisy areas removed.

CDT Correlation with Noise

We have shown that powerline noise has a small positive correlation with the *x*-axis signal that is also used in the depth transforms (fig. 14c). Powerline noise might also influence depth transforms. We examined this possible influence by calculating the average correlation coefficient between calculated apparent conductivity at 10-m depth intervals between 10 and 290 m for each of the four survey blocks (fig. 16). There is a small, positive correlation between powerline noise and conductivity at shallow depths that corresponds to the small, positive correlation observed at early times in the *x*-axis data. This correlation was determined using all airborne TDEM data and served as the rationale for deleting locations with large powerline noise values from apparent conductivity maps and depth slices.

CDT Comparison with Ground TDEM Models

Preliminary modeling and field measurements using ground-based instruments produced models of apparent conductivity changes with depth at several locations (fig. 8) that can be compared with CDT profiles calculated from airborne data acquired at the same location. Using the series of ground measurements along the southeast boundary of the Pantex Plant as an example (TDEM 1, 6, 5, 7, and 10 from south to north), we extracted all airborne sounding locations within 50 m of the ground-based sounding and plotted the apparent conductivity profiles on the same depth and conductivity scale (fig. 17). The ground-based profiles consist of two to four discrete conductivity layers that were shown to be influenced by changes in thickness of the FGZ and perched aquifer, but could not resolve the FGZ (Paine, 2000). The CDTs derived from airborne data are only generally similar to depth profiles obtained from ground-based data, but may more accurately represent smoother conductivity changes with depth that are apparent from borehole logs.

Plots of CDT profiles near ground-based soundings also help determine the exploration depth achieved by the airborne instruments. In most areas, CDTs derived from locations within a

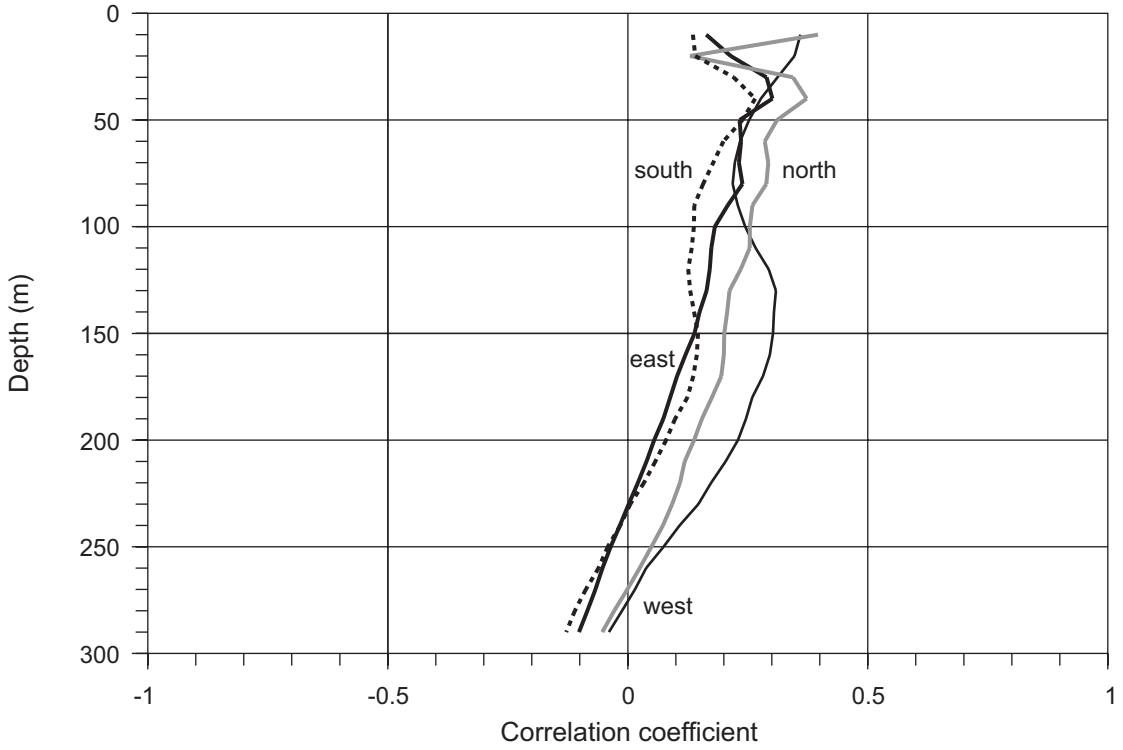

Figure 16. Correlation coefficient between powerline noise and calculated apparent conductivity at specific depths in the north, east, south, and west airborne geophysical survey blocks.

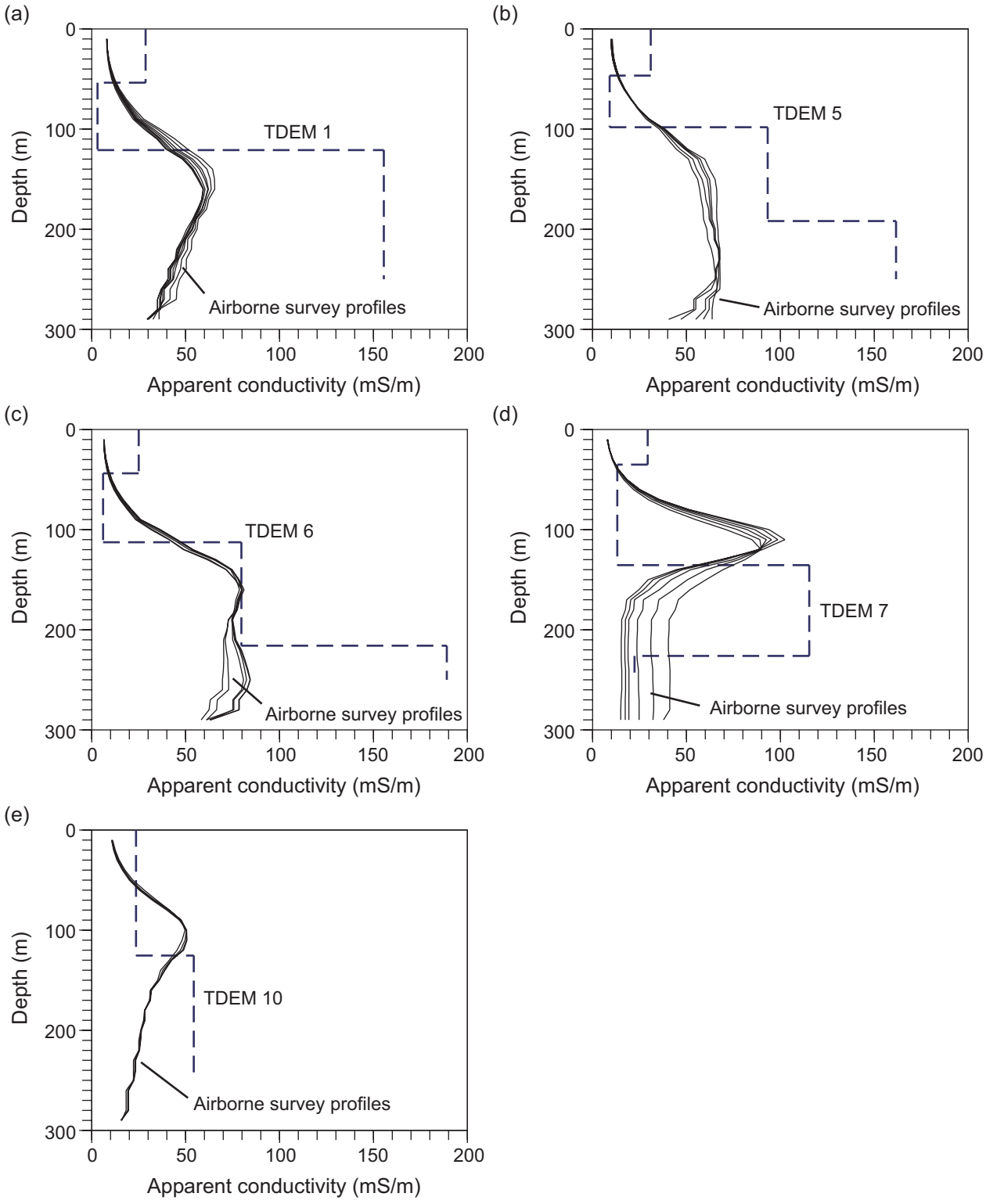

Figure 17. Comparisons between apparent conductivity profiles derived from airborne and ground-based TDEM instruments in the Pantex Southeast area at (a) TDEM 1, (b) TDEM 5, (c) TDEM 6, (d) TDEM 7, and (e) TDEM 10. Locations shown on fig. 8. Airborne profiles are those from all sites within 50 m of the location of the ground-based sounding.

few tens of meters of each other should depict similar profiles, given the large sampling footprint of the airborne system. CDTs from locations near TDEM 1 have similar apparent conductivity values at all depths (fig. 17a), as do those from locations near TDEM 10 (fig. 17e). Profiles near TDEM 6 diverge at depths greater than 180 m (fig. 17c), suggesting that apparent conductivity data deeper than 180 m at this location are unreliable. CDTs near TDEM 5 begin to diverge below 100 m, becoming strongly divergent below 250 m depth (fig. 17b). CDTs near TDEM 7 show increasing divergence at depths greater than 140 m. Possible reasons for divergence include differing transmitter and receiver geometries, powerline noise, and signal strength.

Apparent Conductivity-Depth Slices from CDTs

Once excessively noisy data have been removed from the airborne TDEM data set, the remaining CDTs can be combined to form a pseudo-three-dimensional apparent conductivity model for the survey area that consists of individual apparent conductivity values at 10-m depth intervals at each CDT location. Although the vertical resolution of TDEM data is limited, the abundance and close spacing of measurements acquired during the airborne survey allow the conductivity volume to be sliced horizontally to produce images depicting apparent conductivity variations across the survey area at specific depths. These values are unlikely to be the true electrical conductivity of the ground at a particular location and depth; rather, they depict relative and semi-quantitative values that should be consistent with surrounding values at the same depths. These images can be helpful in identifying geologic and hydrologic features associated with conductivity changes related to differing clay and water content.

Features of special interest in the Pantex Plant area include the unsaturated zone above the perched aquifer, the FGZ and perched aquifer, the unsaturated zone between the FGZ and the main Ogallala aquifer, and the Ogallala aquifer. Numerous wells, borings, and water-level measurements indicate relevant depth ranges for each of these features (fig. 18). Reported water levels for the perched aquifer range from 52 to 90 m, averaging about 80 m. The top of the FGZ

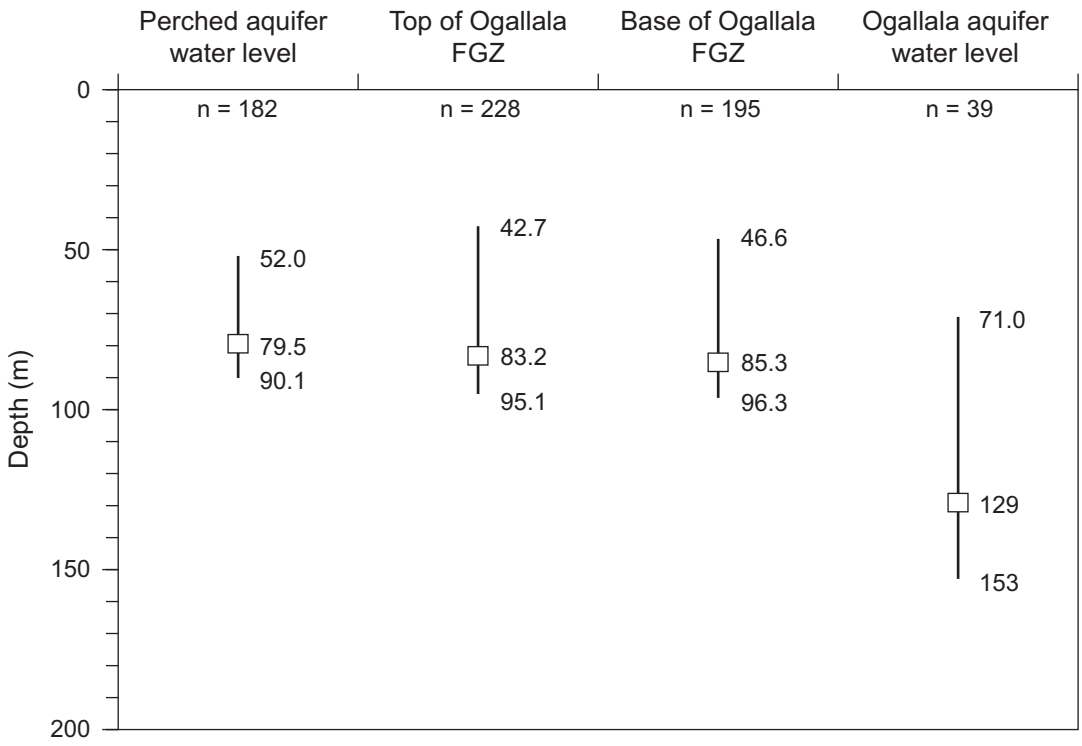

Figure 18. Minimum, maximum, and average reported depths of the perched aquifer water level, the top of the FGZ, the base of the FGZ, and the Ogallala water level. Data from BWXT Pantex.

has been interpreted to range from as shallow as 43 m to as deep as 95 m, averaging 83 m. The wide range of reported depths to the FGZ suggest that what is being interpreted as the FGZ is not in every case the same stratigraphic interval. The base of the FGZ is poorly constrained because most borings purposely do not extend through it. Reported depths for the base of the FGZ average 85 m, but probably are inaccurate. Ogallala water levels vary across the plant area from 71 to 153 m, averaging 129 m.

We combined CDT profiles from the four survey blocks after deleting profiles with powerline noise above the 15 mV threshold. We produced pseudo-depth slices at 10-m intervals between 10 and 200 m depth (appendix B) that show relative apparent conductivity changes across the survey area. Areas where powerline noise is high or where no data were acquired are shown in black.

At this preliminary stage of analysis, we chose the 40 m depth slice to represent the unsaturated zone above the perched aquifer (figs. 19 and B4), the 80 m depth slice to represent the perched aquifer and FGZ (figs. 20 and B8), the 120 m depth slice to represent the unsaturated zone above the Ogallala aquifer (figs. 21 and B12), and the 160 m depth slice to represent the lower Ogallala Formation and pre-Ogallala deposits (fig. 22 and B16).

At the 40 m depth, representing the dominantly unsaturated Ogallala sediments above the perched aquifer, apparent conductivities are relatively low (figs. 17, 19, and B4). Most apparent conductivities at this depth are between 3 and 27 mS/m. Relatively high conductivities suggesting clayey or wet strata are found at each of the survey area playas, consistent with a model of lacustrine playa deposition and local water saturation. High apparent conductivities also appear in the southwest part of the survey area that are at least partly coincident with power lines, buildings, and other cultural features. These are likely to be cultural artifacts that may be removable with further processing. Relatively low apparent conductivities surround the playas, suggesting the presence of coarser and drier strata beneath the upland, interplaya surface. Although no conductivity data are available at Playa 1, elevated conductivities extend east of this playa (fig. 19). Enhanced groundwater recharge at this playa that has contributed to the presence of a

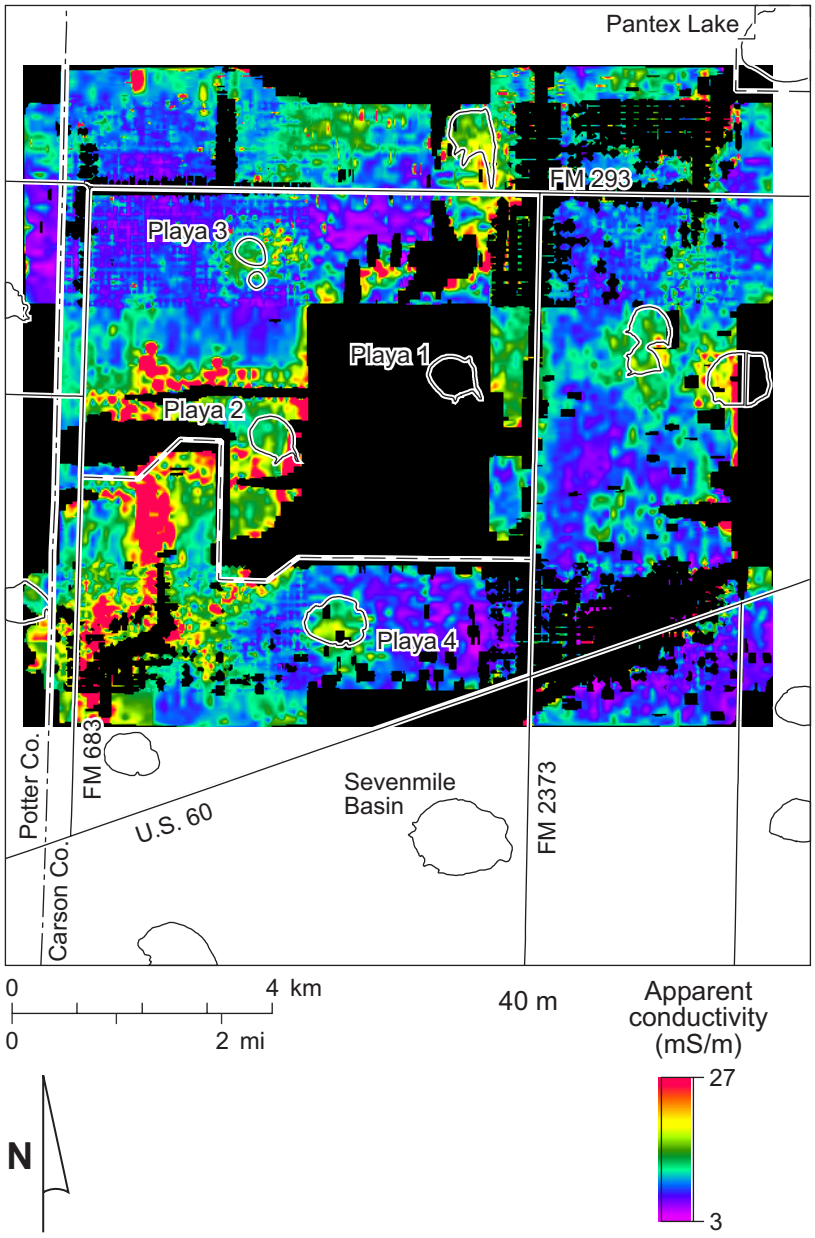

Figure 19. Apparent conductivity at 40 m depth (upper Ogallala Formation above the perched aquifer).

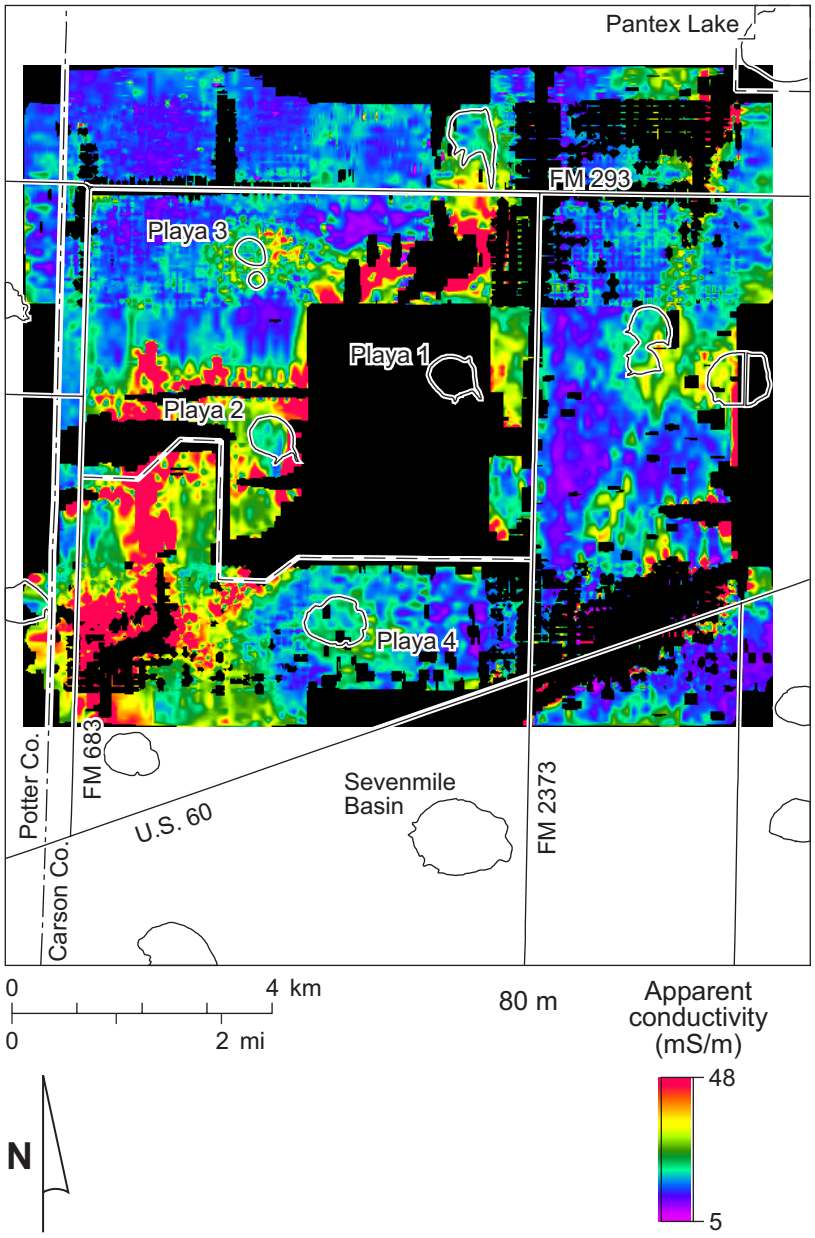

Figure 20. Apparent conductivity at 80 m depth (approximate depth of the perched aquifer and FGZ).

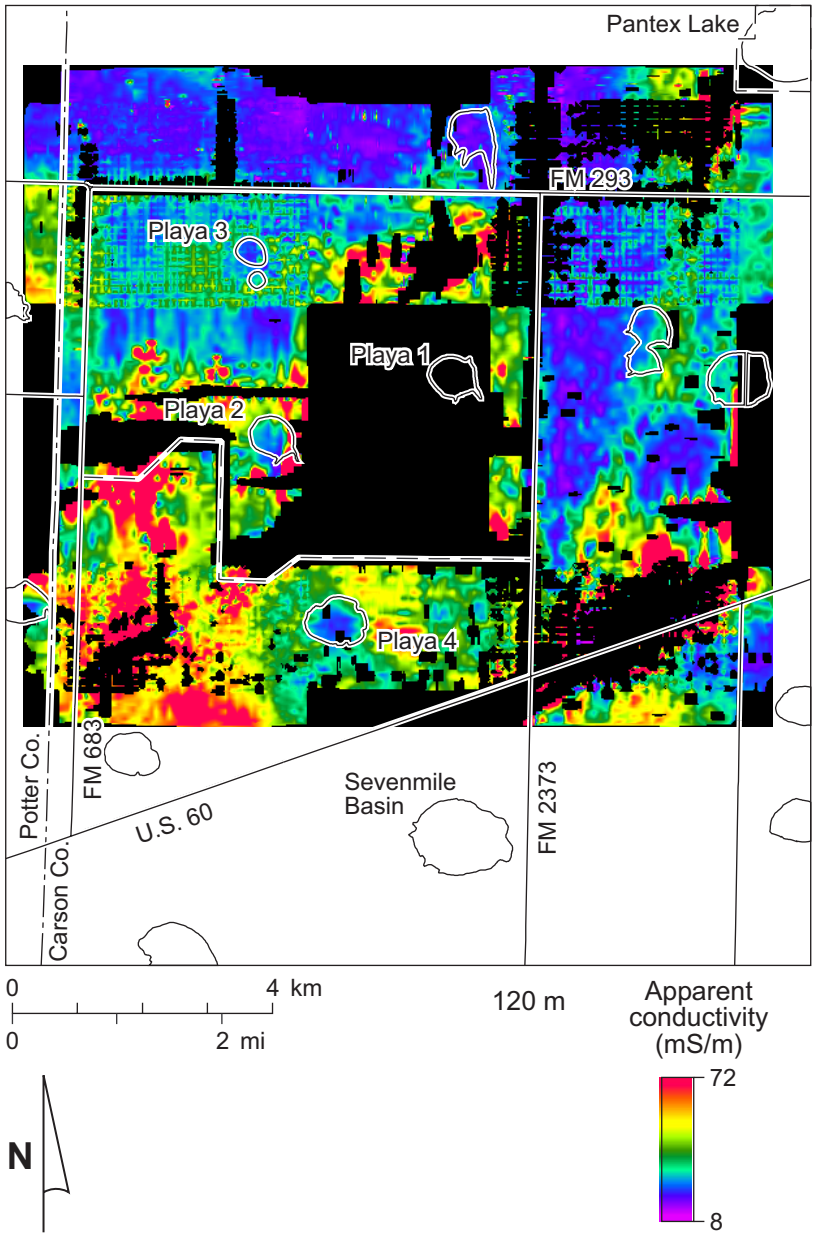

Figure 21. Apparent conductivity at 120 m depth (below the perched aquifer and above the Ogallala aquifer).

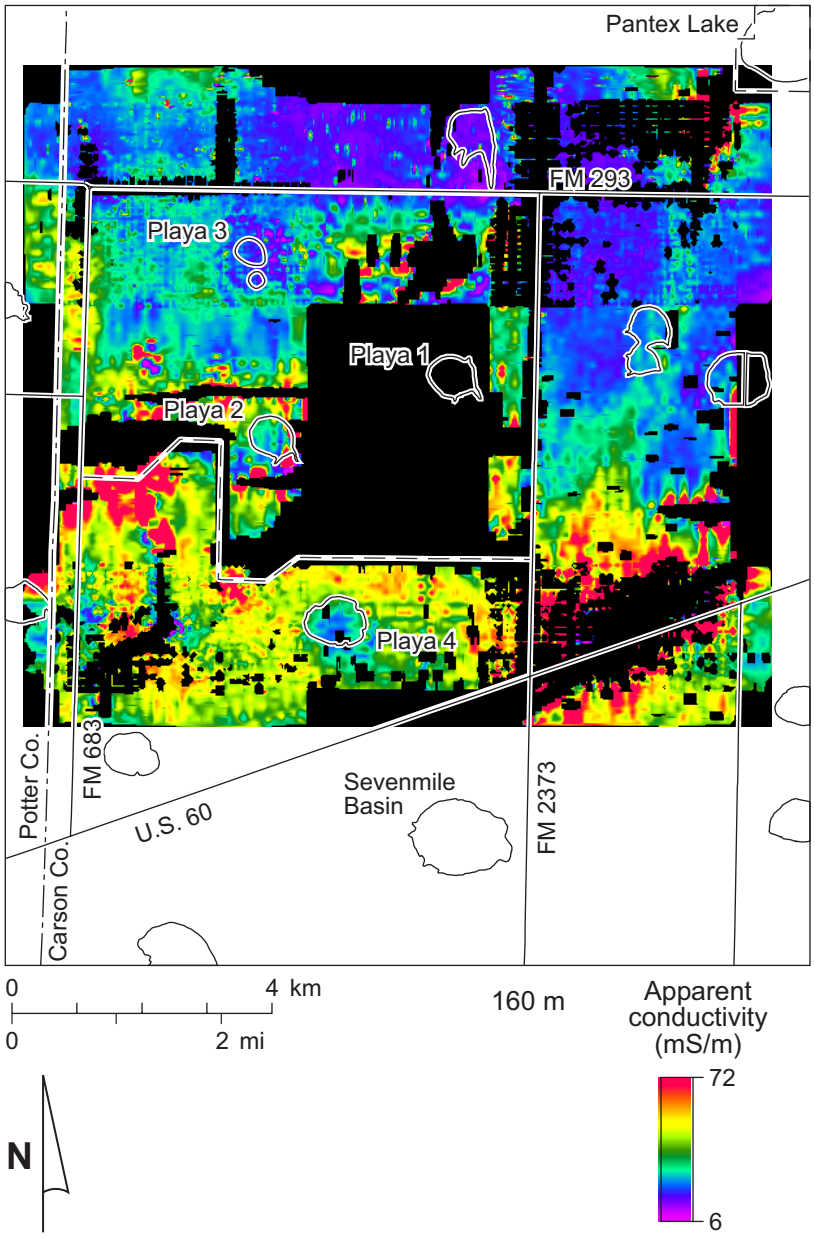

Figure 22. Apparent conductivity at 160 m depth (below the Ogallala water level in the lower Ogallala Formation or underlying Permian or Triassic deposits).

perched aquifer mound may have also increased water content surrounding the playa at shallower depths.

The 80 m depth slice (fig. 20 and B8) is at the approximate depth of the perched aquifer and FGZ. At this depth, apparent conductivities are generally higher than those at shallower depths, ranging from 5 to 48 mS/m. These elevated conductivities suggest higher moisture and perhaps clay contents than in shallower strata. Artifactual conductivity highs are evident in the southwestern part of the survey area and along the pipelines in the east block (fig. 11). A curvilinear conductivity high of uncertain origin trends northward along the east flank of Playa 2, bending eastward as it enters the north block northwest of Playa 1 (fig. 20). Relative conductivity highs are not as evident beneath the playas at this depth. A gentle high occurs at and near Playas 3 and 4, the unnamed playa on the east margin of the survey area, and surrounding Playa 1, but relative lows are depicted at Playa 2 and the Pratt playa. Apparent conductivity highs at this depth are likely to be caused by a thickened perched aquifer or FGZ.

By the 120 m depth (figs. 21 and B12), broadly representing the stratigraphic zone beneath the FGZ and above the Ogallala aquifer, all the surveyed playas coincide with pronounced apparent conductivity lows. In general, apparent conductivity values at this depth are higher than those at shallower depths; most values are between 8 and 72 mS/m. Elevated apparent conductivities are present on all sides of the main Pantex Plant. It is not clear yet whether these high areas might reflect increased clay or water content at this depth around the plant, or whether the elevated conductivities are an artifact of abundant cultural noise at the plant.

The 160 m depth slice (figs. 22 and B16) represents the interval at or below the Ogallala water level. Apparent conductivities remain relatively high at this depth, ranging from 6 to 72 mS/m after removal of noisy CDT profiles. Pronounced conductivity lows persist beneath the playas. An extensive area of relatively low conductivity is present north and northwest of the Pantex Plant that encompasses part of the City of Amarillo Ogallala water well field, where Ogallala deposits are thickest. Higher apparent conductivities in the southwest part of the study

area at these and deeper depths may be caused by fine-grained Permian or Triassic strata underlying the Ogallala Formation.

FOCUS AREAS

In the initial part of this study summarized in this interim report, we primarily examined suvey-wide geophysical data and have not yet integrated available geological and hydrological data. In addition to the survey-wide data, we have concentrated efforts on several focus areas, including Playa 3, the old Sewage Treatment Plant (OSTP) area, and southeast of the Pantex Plant (fig. 23). To date, we have extracted CDT profiles from the airborne geophysical data set for these areas and are examining each in more detail than is possible at the survey-wide scale. Work to be done in these and other areas includes integrating the geophysical results with other subsurface information.

Playa 3

The Playa 3 focus area (figs. 23 and 24) is a 2.4 x 2.4 km area northwest of the Pantex Plant that encompasses Playa 3, its enclosing basin, and the Burning Grounds. Numerous wells and borings have been drilled, although none penetrate the playa floor. Most of the focus area falls within both the west and north airborne survey blocks (figs. 1 and 8), resulting in coverage along north–south and east–west flight lines. Seismic data were acquired across this playa in 1993 that showed there was evidence of playa formation by dissolution-induced subsidence (Paine, 1995). Reconnaissance, ground-based TDEM soundings acquired in 2000 showed that strata beneath the playa floor are more conductive at shallow depths and less conductive at greater depths than strata at similar depths outside the playa basin (Paine, 2000), consistent with a collapse model of playa formation. The collapse model may have significant implications regarding the continuity of the FGZ beneath Pantex playas.

Figure 23. Map showing Playa 3, OSTP, and Southeast focus areas.

Detailed ground elevation data from the airborne geophysical survey clearly show the low basin adjacent to the Burning Grounds that encloses Playa 3 and it southerly sub-playa (fig. 25). Elevation ranges from 1080 to 1096 m; there is 10 m or more of surface relief between the playa floor and the surrounding interplaya surface. The playa itself covers a relatively small part of the larger playa basin.

Selected conductivity-depth slices at Playa 3 are consistent with the results of the ground TDEM measurements and seismic data. At a depth of 40 m, which represents upper Ogallala Formation deposits in interplaya areas and is above the perched aquifer and FGZ (fig. 18), the apparent conductivity image depicts highest conductivities beneath the basin enclosing Playa 3 (fig. 26). Areas of low apparent conductivity surround the basin. High apparent conductivities are also shown at the Burning Grounds, but the presence of several individual peaks suggests that the elevated conductivities here are at least partly an artifact of metallic structures or perhaps power lines. Elevated conductivities beneath the playa basin are consistent with higher clay and water content of lacustrine deposits filling the basin. Outside the basin, lower apparent conductivities are consistent with the presence of coarser and drier upper Ogallala fluvial deposits described in nearby wells and borings.

Apparent conductivities remain elevated beneath the playa basin at 80 m depth (fig. 27), but are less pronounced and cover a slightly larger area around the playa. This is the approximate depth of the perched aquifer and FGZ in other parts of the plant (fig. 18). Prominent conductivity lows northeast of the Burning Grounds and south of Playa 3 are separated by a zone of elevated apparent conductivity that trends east-southeast from Playa 3. These elevated conductivities may delineate areas of thicker FGZ development or higher water content.

The depth slice at 120 m depicts apparent conductivity within the middle to lower Ogallala Formation, below the FGZ and above the Ogallala water level (fig. 28). The most prominent feature is the pronounced conductivity low that coincides with Playa 3; higher apparent conductivities surround the playa beneath the interplaya surface. Low apparent conductivities beneath the playa are consistent with an interpretation of the playa as a subsidence and collapse feature.

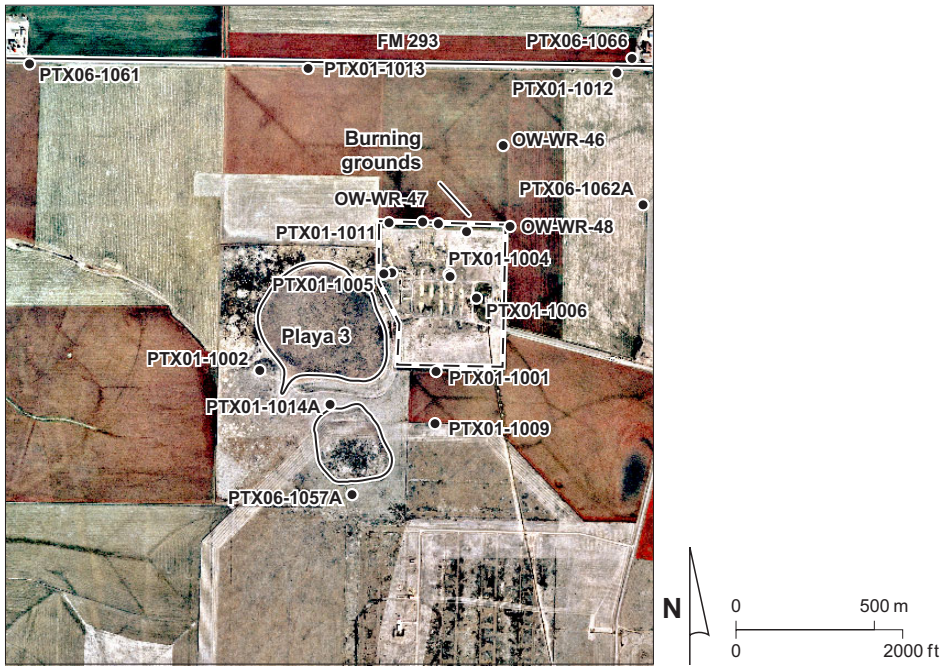

Figure 24. Aerial photograph of Playa 3 and the Burning Grounds. Also shown are well and boring locations.

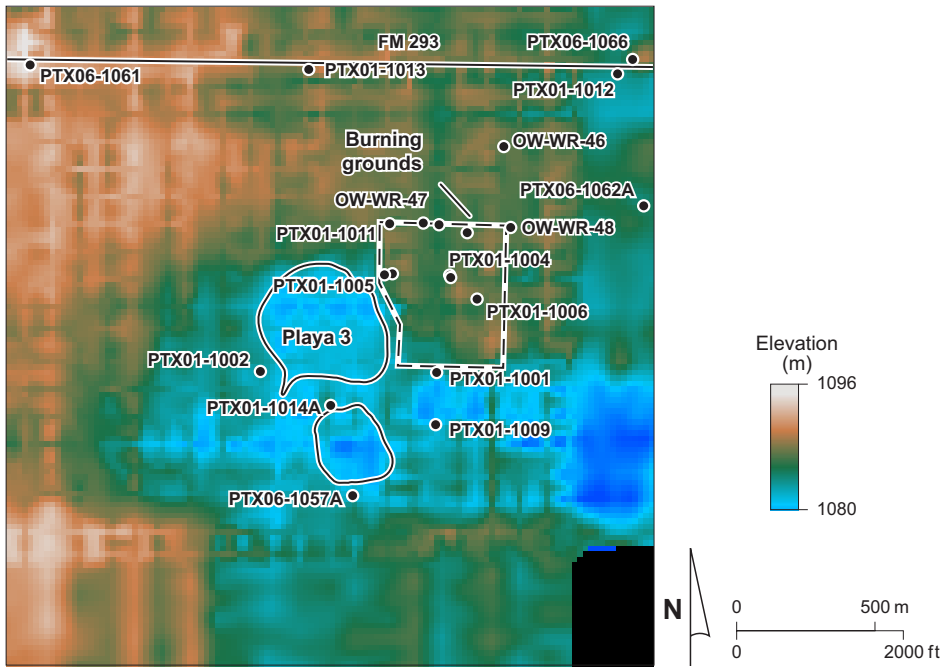

Figure 25. Terrain map of Playa 3 and the Burning Grounds. Also shown are well and boring locations.

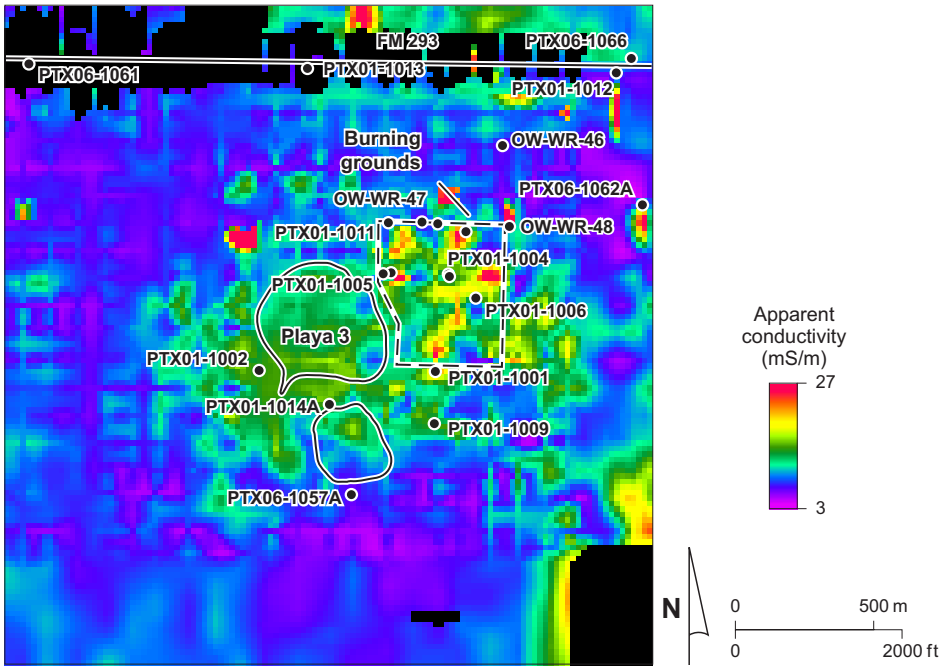

Figure 26. Apparent conductivity at 40 m depth in the Playa 3 focus area.

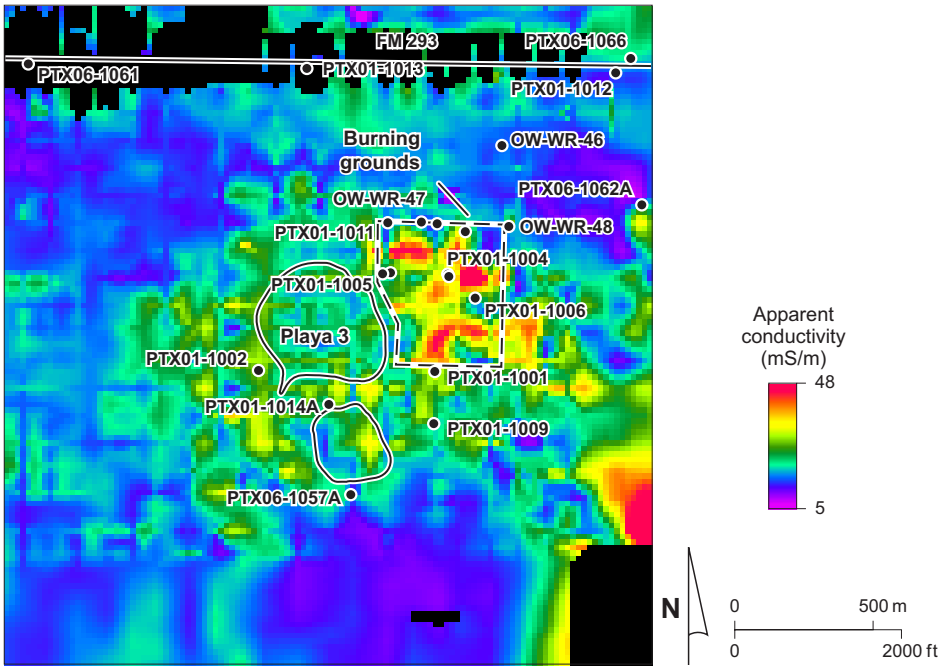

Figure 27. Apparent conductivity at 80 m depth in the Playa 3 focus area.

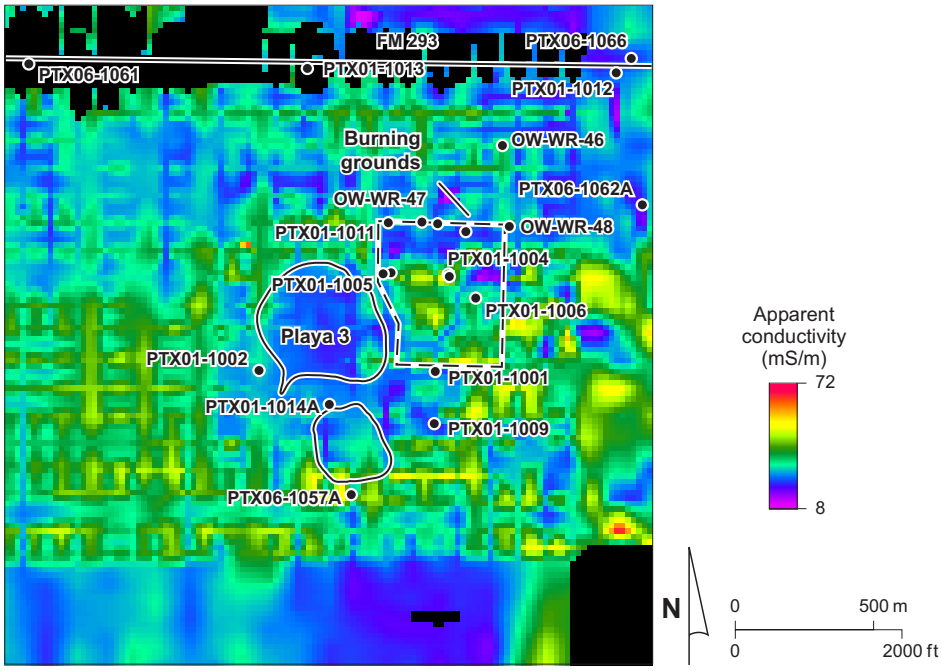

Figure 28. Apparent conductivity at 120 m depth in the Playa 3 focus area.

At this depth, lower conductivities could be caused by higher porosity developed through collapse and brecciation.

Pantex Southeast

The thickness of the FGZ and saturated thickness of the perched aquifer are acute issues related to lateral and vertical migration of contaminants in the perched aquifer at Pantex, particularly in the Southeast focus area (fig. 23). The Pantex Southeast focus area, measuring 3.2 km east–west and 3 km north–south, encompasses numerous borings and wells (fig. 29). North–south flight lines in the east block cover the entire focus area; east–west flight lines in the south block give double coverage along the south edge (figs. 1 and 8).

Cultural noise is a problem in this area. EM noise generated by major and minor power lines is strong along FM 2373, the Pantex east gate entrance road, the southern boundary of the Pantex Plant, and U.S. 60 near the southeast corner of the focus area (fig. 12). Powerline noise exceeds the 15 mV threshold along all of these features, significantly reducing the number of CDTs available to produce conductivity-depth slices. Additionally, a major pipeline crosses from southwest to northeast and is clearly visible on depth slices deeper than about 50 m (appendix B). Pump-and-treat infrastructure, including wellheads, metallic pipes, structures, and electrical lines may also contribute to cultural contamination of the EM signal.

Despite these difficulties, apparent conductivity trends are visible on depth slices of the Pantex Southeast area. Above the FGZ and perched aquifer, maps of apparent conductivity at 40 m depth depict mostly low values east of FM 2373 (fig. 30), consistent with relatively coarse and unsaturated upper Ogallala Formation fluvial deposits. Higher apparent conductivities are found locally along the northeast-trending pipeline that are probably cultural artifacts. At the approximate depth of the perched aquifer and FGZ at 80 m (fig. 31), apparent conductivities remain low within the concentration of wells and borings east of FM 2373, suggesting thin or absent perched aquifer and associated FGZ deposits. Elevated apparent conductivities in the

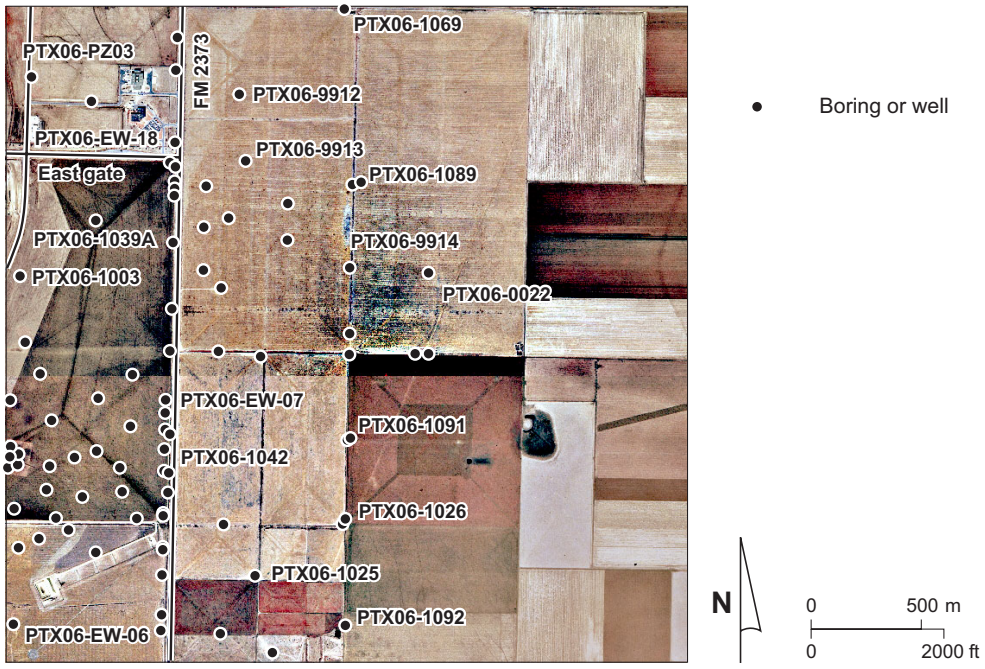

Figure 29. Aerial photograph of Pantex Southeast focus area. Also shown are well and boring locations.

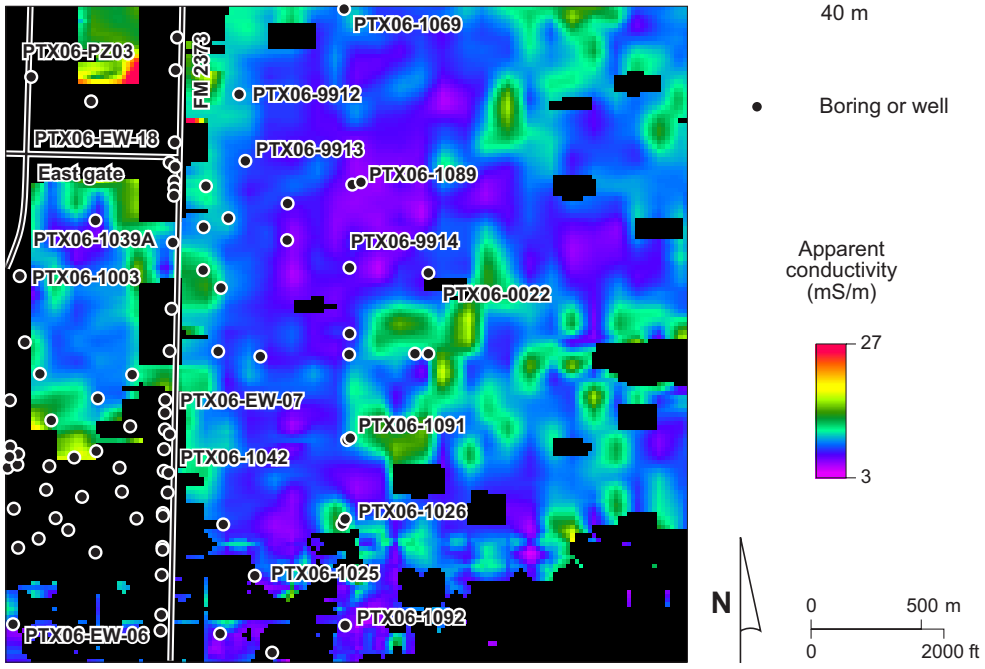

Figure 30. Apparent conductivity at 40 m depth in the Pantex Southeast focus area.

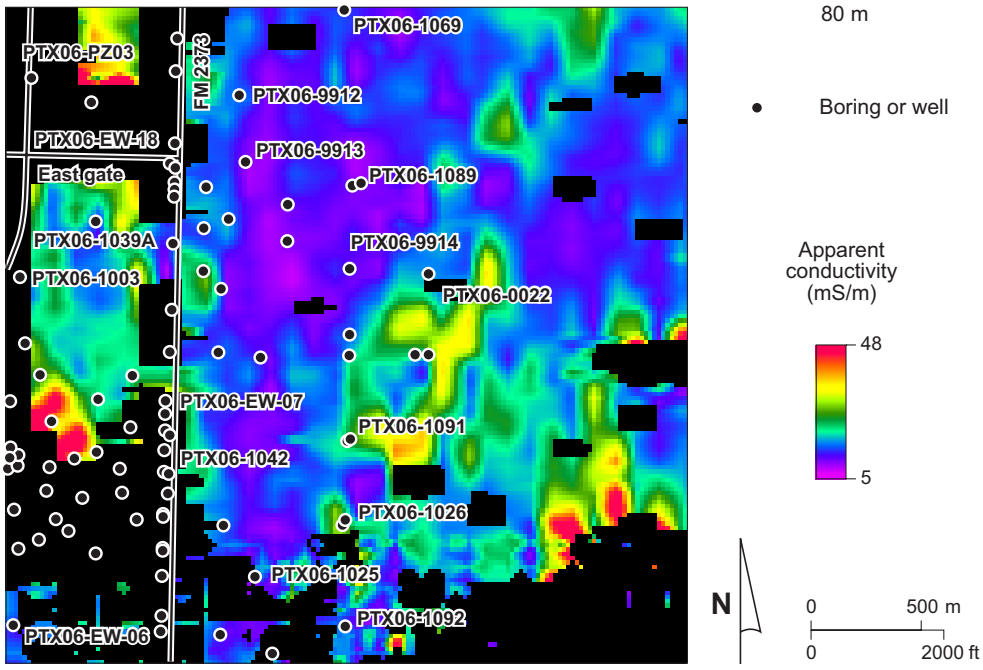

Figure 31. Apparent conductivity at 80 m depth in the Pantex Southeast focus area.

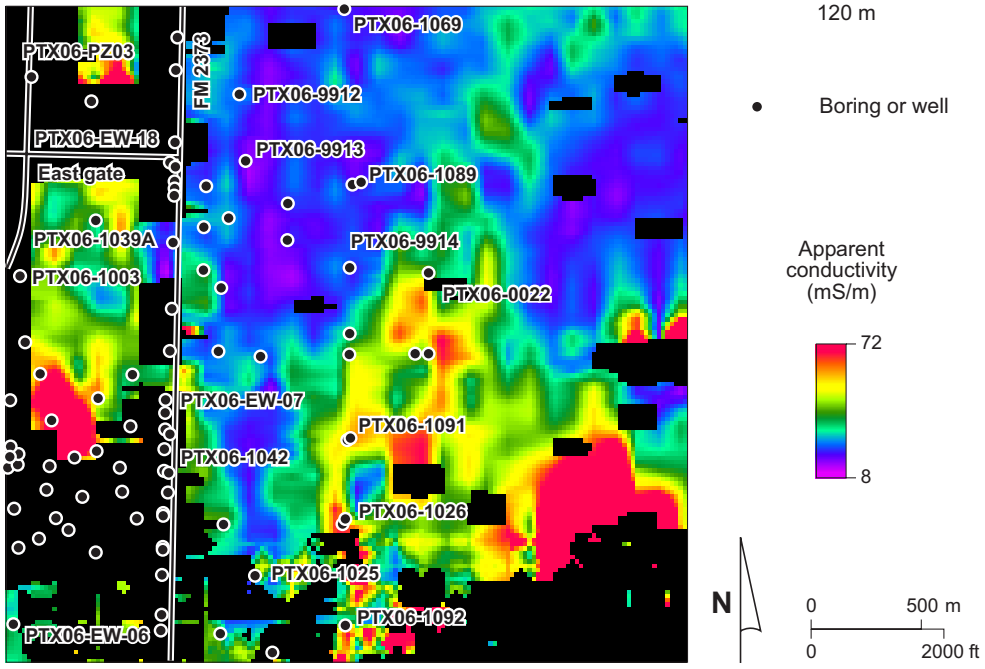

Figure 32. Apparent conductivity at 120 m depth in the Pantex Southeast focus area.

northwest corner of the focus area appear to be related to the elevated conductivities surrounding Playa 1 (fig. 20), reflecting a thickened FGZ and perched aquifer. Apparent conductivities are also elevated along and southwest of a line joining wells PTX06-1003 and PTX06-EW-07 (fig. 31). This zone of elevated apparent conductivity extends southeastward across FM 2373 a short distance. Elevated conductivities at this depth are likely to be caused by increases in FGZ thickness or perched aquifer saturated thickness. The low apparent conductivities east of FM 2373 suggest a thin or absent FGZ and perched aquifer.

At a depth of 120 m, situated within the Ogallala Formation below the FGZ and above the Ogallala water level, apparent conductivities are generally higher than they are at shallower depths (fig. 32). Elevated apparent conductivities persist and expand in areal coverage on the Pantex Plant and extend a short distance east of FM 2373 in some places. Because the effect of noise increases as EM signal strength decreases with depth, these elevated apparent conductivities could be an artifact of cultural noise. If real, it could be that Ogallala strata beneath the FGZ have higher clay or water content beneath the perched aquifer, implying possible downward water migration through the FGZ in this area. This important issue will be investigated further when well and boring data are integrated with the geophysical data.

CONCLUSIONS AND REMAINING TASKS

This interim report summarizes work to date on the airborne geophysical survey of the Pantex Plant area completed in March 2003, which is being used to assess the integrity and extent of the FGZ on and near the Pantex Plant. High resolution airborne geophysical data, including TDEM and magnetic field data, were acquired over four survey blocks surrounding the Pantex Plant and were processed to produce models of apparent conductivity changes with depth. We achieved exploration depths to the lower Ogallala Formation and perhaps to pre-Ogallala strata where the Ogallala is relatively thin. Analysis of powerline and other cultural noise related to pipelines and structures resulted in the removal of about 20 percent of the 104,880 measure-

ment locations from the final TDEM data set. Comparisons of apparent conductivity profiles derived from ground and airborne instruments showed general agreement in magnitude and shape; smoothly varying profiles derived from airborne data are more realistic approximations of the actual electrical conductivity of the ground. We constructed conductivity-depth slices depicting apparent electrical conductivity across the survey area from the remaining measurement locations at 10-m intervals between depths of 10 and 200 m below the ground surface. We are analyzing these images to interpret geological and hydrological features related to the perched aquifer, FGZ, and the Ogallala aquifer.

Representative conductivity-depth images for strata above the perched aquifer (40 m depth), at the approximate depth of the perched aquifer and FGZ (80 m), between the FGZ and Ogallala aquifer (120 m), and below the Ogallala water table (160 m) reveal patterns that can be used to interpret changes in clay and water content that are relevant to groundwater flow. Conductivity images of the subsurface beneath survey-area playas are consistent with a playa formation model of dissolution-induced subsidence and lacustrine fill. Elevated apparent conductivities associated with the Pantex Southeast perched aquifer plume appear to extend a short distance beyond the plant boundary at FM 2373 and may continue below the FGZ in places.

Tasks remaining before the project is complete include (1) integrate available geologic and hydrologic data from wells and borings with results from the airborne geophysical survey; (2) analyze the influence of the FGZ and variations in perched aquifer saturated thickness on apparent conductivities measured during the airborne geophysical survey; (3) resolve the interpretational ambiguity between hydrogeological influences and cultural noise in critical areas; (4) use combined hydrogeological and geophysical data to evaluate the integrity and extent of the FGZ, the potential for groundwater flow through thin or absent FGZ, and the groundwater implications of anomalous conductivity profiles observed at the playas; and (5) prepare a final report summarizing project results.

ACKNOWLEDGMENTS

This project is funded by BWXT Pantex under contract number 00026424 between The University of Texas at Austin and BWXT Pantex. S. Todd Harris of BWXT Pantex is the project manager. BWXT staff Todd Harris, Shane Currie, and Jeffrey Stovall provided geological and hydrological data. James Phelan and Carolyn Byrd of Sandia National Laboratories assisted in project justification and airborne survey approval. Fugro Airborne Surveys staff Darcy Wiens, Mark Williston, and Renko Constapel flew and maintained the aircraft, Dave Patzer operated onboard instruments, and Rick Williams and Brenda Sharp processed the data. We appreciate the management at Pantex, both BWXT and DOE, for their assistance in approving the project despite safety and security concerns.

REFERENCES

Frischknecht, F. C., Labson, V. F., Spies, B. R., and Anderson, W. L., 1991, Profiling using small sources, *in* Nabighian, M. N., ed., Electromagnetic methods in applied geophysics – applications, part A and part B: Tulsa, Society of Exploration Geophysicists, p. 105-270.

Fugro Airborne Surveys, 2003, Logistics and processing report: airborne magnetic and GEOTEM survey, Pantex survey area, Amarillo, Texas, USA: Fugro Airborne Surveys, Ottawa, Ontario, Canada, Job No. 03428, 73 p.

Geonics Limited, 1992, Protem 47 operating manual: Mississauga, Ontario, variously paginated.

Gustavson, T. C., Bebout, D. G., Bennett, P. C., Fish, E. B., Fryar, A. E., Hovorka, S. D., Hua, Hsiao-Peng, Kirschenmann, Kyle, Laun, Scot, Minehardt, T. J., Mullican, W. F., III, Nicot, Jean-Philippe, Paine, J. G., Pezzolesi, T. P., Rainwater, Ken, Ramsey, Heyward, Reedüer, Alan, Romanak, K. D., Scanlon, B. R., Thompson, David, Xiang, Jiannan, Zartman, R. E., 1995, Summary hydrogeologic assessment, U.S. Department of Energy Pantex Plant,

Carson County, Texas: The University of Texas at Austin, Bureau of Economic Geology, contract report prepared for the U.S. Department of Energy, 127 p.

Kaufman, A. A., and Keller, G. V., 1983, Frequency and transient soundings: Elsevier, Amsterdam, Methods in Geochemistry and Geophysics, No. 16, 685 p.

Paine, J. G., 1995, Shallow-seismic evidence for playa basin development by dissolution-induced subsidence on the Southern High Plains, Texas: The University of Texas at Austin, Bureau of Economic Geology Report of Investigations 233, 47 p.

Paine, J. G., 2000, Seismic evaluation and reconnaissance TDEM survey of the Southeast and Playa 3 areas of the Pantex Plant, Carson County, Texas: The University of Texas at Austin, Bureau of Economic Geology, report prepared for the Innovative Treatment Remediation Demonstration Program, Sandia National Laboratories under P.O. document no. 12236, 51 p.

Pantex Plant Environmental Restoration Department, 2000, Groundwater program management action process: final report prepared for the U.S. Department of Energy under subcontract 16189, June 2000, not consecutively paginated.

Parasnis, D. S., 1973, Mining geophysics: Amsterdam, Elsevier, 395 p.

Parasnis, D. S., 1986, Principles of applied geophysics: Chapman and Hall, 402 p.

Smith, R. S., and Annan, A. P., 2000, Using an induction coil sensor to indirectly measure the B-field response in the bandwidth of the transient electromagnetic method: Geophysics, v. 65, no. 5, p. 1489-1494.

Spies, B. R., and Frischknecht, F. C., 1991, Electromagnetic sounding: *in* Nabighian, M. N., ed., Electromagnetic methods in applied geophysics – applications, part A and part B: Tulsa, Society of Exploration Geophysicists, p. 285-386.

U.S. Army Corps of Engineers, Tulsa District, 1992, U.S. Department of Energy Pantex Plant: Amarillo, Texas, hydrogeological assessment, variously paginated.

U.S. Department of Energy, Technical Assistance Team, 2000, Protecting the Ogallala aquifer II: recommendations for characterization and remediation of the southeastern plume at the Pantex Plant: final report, July 7, 2000, 21 p.

West, G. F., and Macnae, J. C., 1991, Physics of the electromagnetic induction exploration method, *in* Nabighian, M. N., ed., Electromagnetic methods in applied geophysics – applications, part A and part B: Tulsa, Society of Exploration Geophysicists, p. 5-45.

Wolfgram, Peter, and Karlik, Gulcin, 1995, Conductivity-depth transform of GEOTEM data: Exploration Geophysics, v. 26, p. 179-185.

APPENDIX A: GROUND-BASED TDEM SOUNDINGS

Locations and best-fit models for ground-based TDEM soundings (Paine, 2000). Locations on fig. 5. Location coordinates given in Universal Transverse Mercator projection, zone 14 north, North American Datum of 1983. Locations derived from differential GPS.

TDEM 1

Date: September 19, 2000
UTM coordinates: x = 268827.54 m, y = 3908688.90 m
Surface elevation: 1073.15 m MSL

Best-fit model (fitting error 3.8 %)

Layer	Resistivity (ohm-m)	Thickness (m)	Conductivity (mS/m)	Top (m)	Base (m)	Top elev. (m)	Base elev. (m)
1	34.9	53.7	28.7	0.0	53.7	1073.2	1019.4
2	324.4	67.3	3.1	53.7	121.0	1019.4	952.2
3	6.4	155.5	121.0			952.2	

TDEM 2

Date: September 19, 2000
UTM coordinates: x = 264595.60 m, y = 3914359.72 m
Surface elevation: 1083.19 m MSL

Best-fit model (fitting error 1.5 %)

Layer	Resistivity (ohm-m)	Thickness (m)	Conductivity (mS/m)	Top (m)	Base (m)	Top elev. (m)	Base elev. (m)
1	9.3	24.8	107.3	0.0	24.8	1083.2	1058.4
2	2374.3	96.8	0.4	24.8	121.6	1058.4	961.6
3	22.1	45.3	121.6			961.6	

TDEM 3

Date: September 19, 2000
UTM coordinates: x = 268185.43 m, y = 3908662.10 m
Surface elevation: 1073.86 m MSL

Best-fit model (fitting error 7.1 %)

Layer	Resistivity (ohm-m)	Thickness (m)	Conductivity (mS/m)	Top (m)	Base (m)	Top elev. (m)	Base elev. (m)
1	21.5	26.7	46.6	0.0	26.7	1073.2	1046.5
2	190.6	84.7	5.2	26.7	111.4	1046.5	961.8
3	15.6	64.0	111.4			961.8	

TDEM 4

Date: September 20, 2000
UTM coordinates: x = 267391.77 m, y = 3908891.22 m
Surface elevation: 1075.71 m MSL

Best-fit model (fitting error 7.9 %)

Layer	Resistivity (ohm-m)	Thickness (m)	Conductivity (mS/m)	Top (m)	Base (m)	Top elev. (m)	Base elev. (m)
1	18.3	19.1	54.6	0.0	19.1	1075.7	1056.6
2	208.1	97.0	4.8	19.1	116.1	1056.6	959.7
3	14.8	67.5	116.1			959.7	

TDEM 5

Date: September 20, 2000
UTM coordinates: x = 268842.06 m, y = 3909356.32 m
Surface elevation: 1075.25 m MSL

Best-fit model (fitting error 3.9 %)

Layer	Resistivity (ohm-m)	Thickness (m)	Conductivity (mS/m)	Top (m)	Base (m)	Top elev. (m)	Base elev. (m)
1	32.3	46.6	30.9	0.0	46.6	1073.2	1026.5
2	110.4	51.5	9.1	46.6	98.1	1026.5	975.0
3	10.7	93.7	93.2	98.1	191.8	975.0	881.3
4	6.2	161.6	191.8			881.3	

TDEM 6

Date: September 20, 2000
UTM coordinates: x = 268783.29 m, y = 3909032.86 m
Surface elevation: 1074.22 m MSL

Best-fit model (fitting error 3.2 %)

Layer	Resistivity (ohm-m)	Thickness (m)	Conductivity (mS/m)	Top (m)	Base (m)	Top elev. (m)	Base elev. (m)
1	40.0	43.8	25.0	0.0	43.8	1074.2	1030.4
2	165.5	68.9	6.0	43.8	112.7	1030.4	961.6
3	12.6	103.3	79.7	112.7	216.0	961.6	858.3
4	5.3	189.0	216.0			858.3	

TDEM 7

Date: September 20, 2000
UTM coordinates: x = 268436.07 m, y = 3910128.05 m
Surface elevation: 1076.71 m MSL

Best-fit model (fitting error 12.1 %)

Layer	Resistivity (ohm-m)	Thickness (m)	Conductivity (mS/m)	Top (m)	Base (m)	Top elev. (m)	Base elev. (m)
1	34.1	35.1	29.3	0.0	35.1	1076.7	1041.7
2	76.2	100.4	13.1	35.1	135.5	1041.7	941.3
3	8.7	90.6	115.3	135.5	226.1	941.3	850.6
4	44.8	22.3	226.1			850.6	

TDEM 8

Date: September 21, 2000
UTM coordinates: x = 265047.28 m, y = 3914231.26 m
Surface elevation: 1087.49 m MSL

Best-fit model (fitting error 1.9 %)

Layer	Resistivity (ohm-m)	Thickness (m)	Conductivity (mS/m)	Top (m)	Base (m)	Top elev. (m)	Base elev. (m)
1	36.5	52.9	27.4	0.0	52.9	1087.5	1034.6
2	329.7	38.8	3.0	52.9	91.7	1034.6	995.8
3	5.7	17.9	174.5	91.7	109.6	995.8	977.9
4	314.1	126.6	3.2	109.6	236.2	977.9	851.3
5	19.1	52.2	236.2			851.3	

TDEM 9

Date: September 21, 2000
UTM coordinates: x = 264289.55 m, y = 3913980.23 m
Surface elevation: 1086.05 m MSL

Best-fit model (fitting error 1.5 %)

Layer	Resistivity (ohm-m)	Thickness (m)	Conductivity (mS/m)	Top (m)	Base (m)	Top elev. (m)	Base elev. (m)
1	24.9	43.1	40.1	0.0	43.1	1086.1	1043.0
2	52.2	113.2	19.2	43.1	156.3	1043.0	929.8
3	16.1	62.3	156.3			929.8	

TDEM 10

Date: September 21, 2000
UTM coordinates: x = 268763.71 m, y = 3911187.08 m
Surface elevation: 1078.43 m MSL

Best-fit model (fitting error 4.0 %)

Layer	Resistivity (ohm-m)	Thickness (m)	Conductivity (mS/m)	Top (m)	Base (m)	Top elev. (m)	Base elev. (m)
1	42.4	125.3	23.6	0.0	125.3	1078.4	953.1
2	18.4	54.3	125.3			953.1	

APPENDIX B: CONDUCTIVITY-DEPTH SLICES

Page intentionally blank

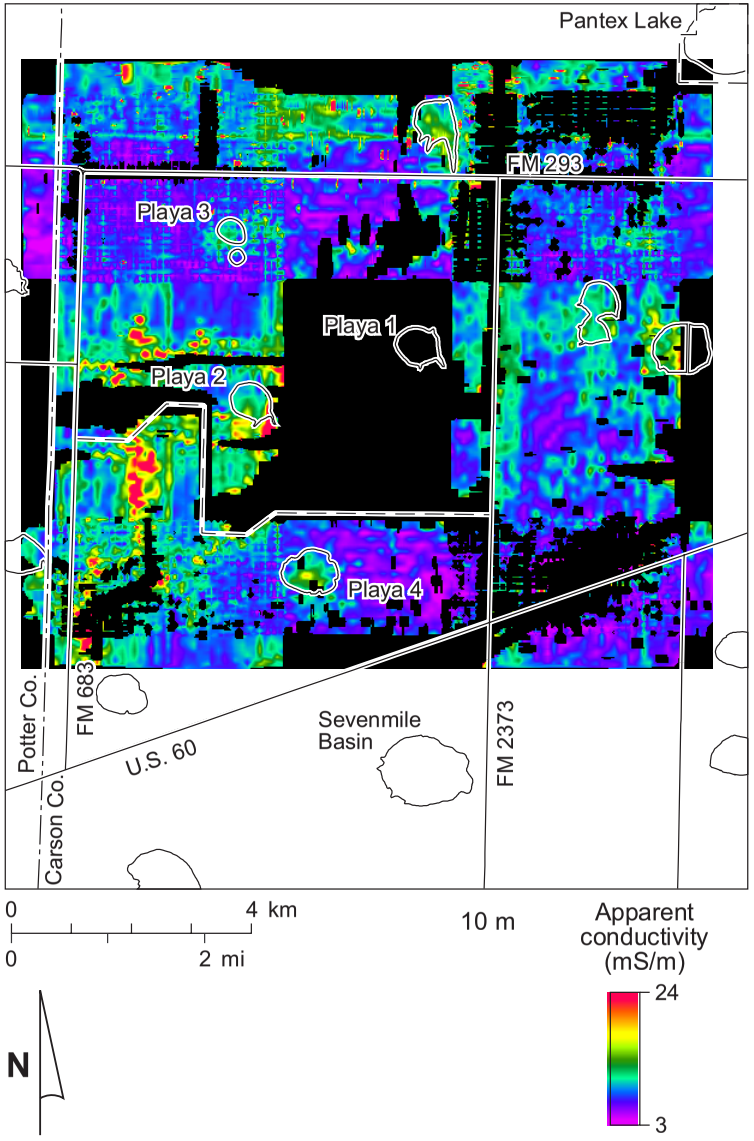

Figure B1. Apparent conductivity at a depth of 10 m.

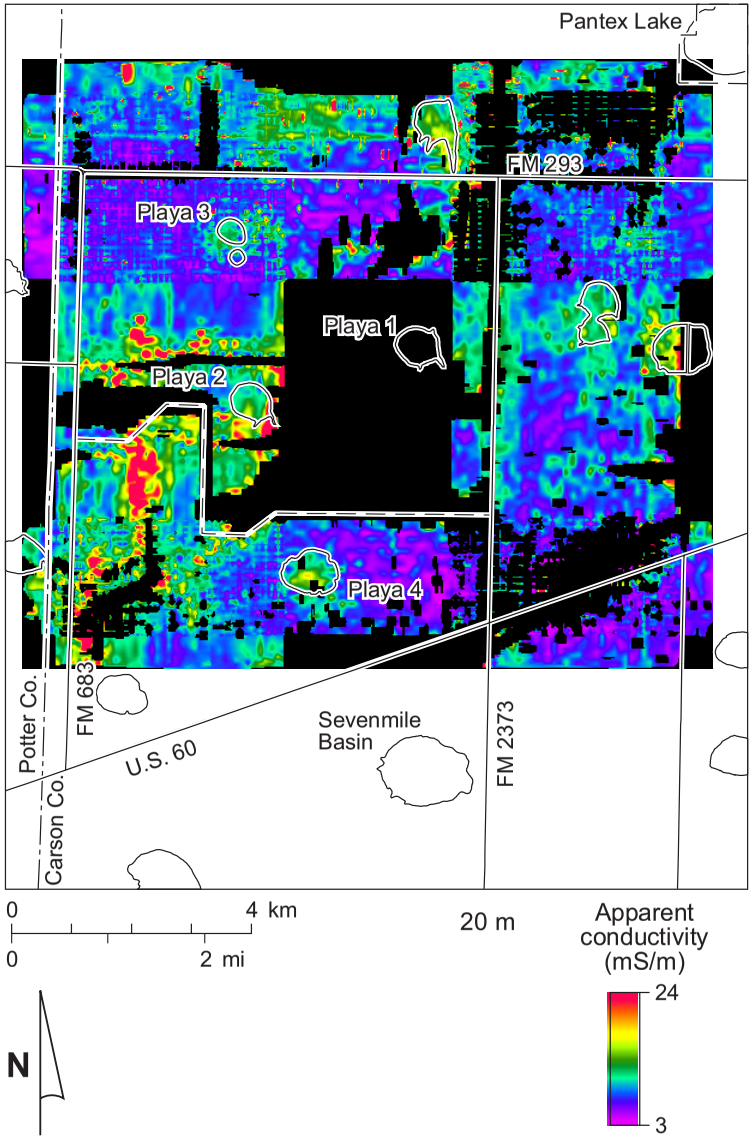

Figure B2. Apparent conductivity at a depth of 20 m.

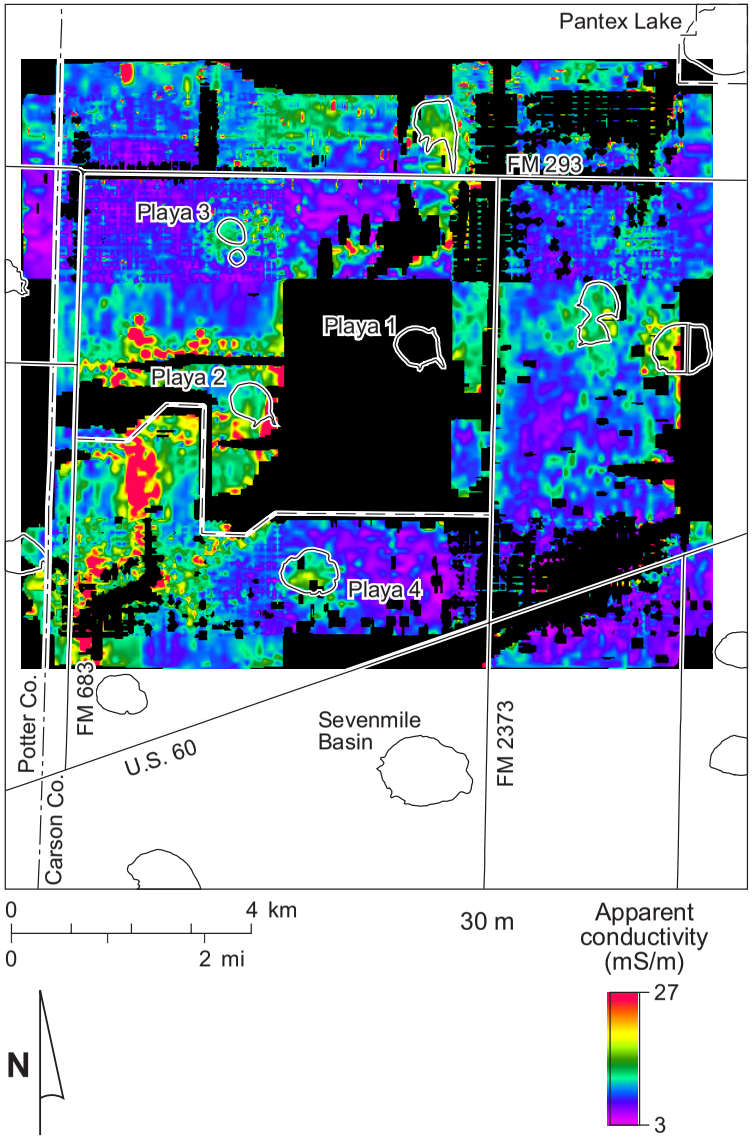

Figure B3. Apparent conductivity at a depth of 30 m.

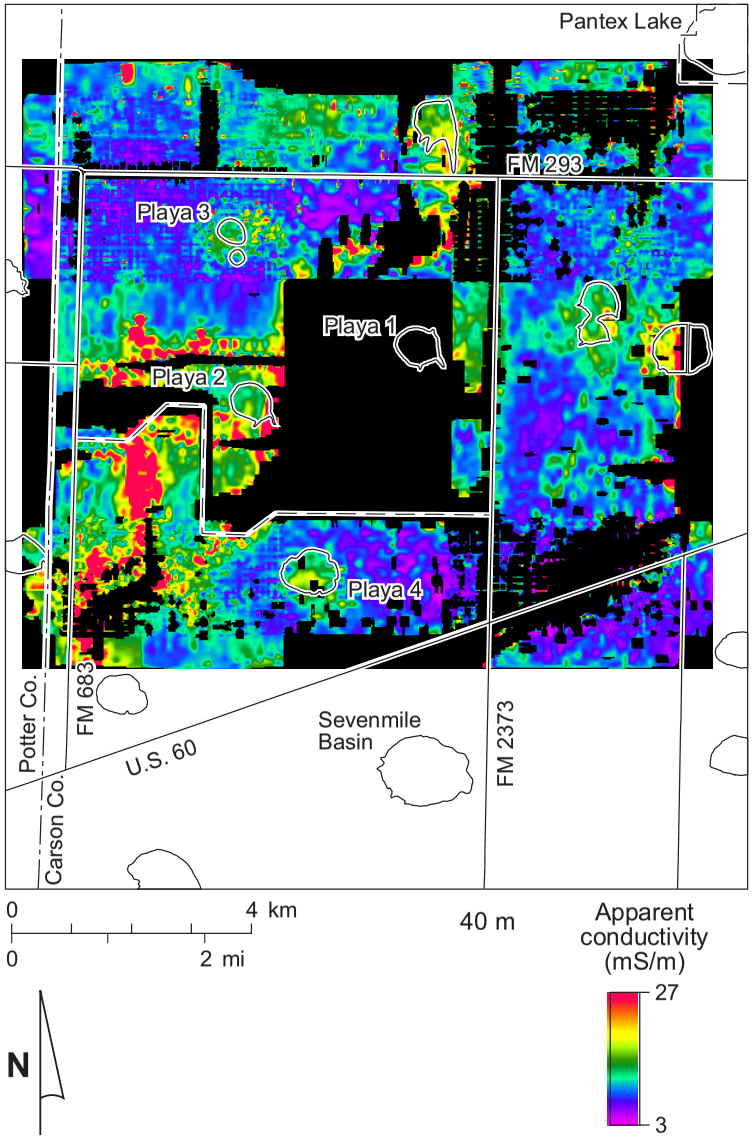

Figure B4. Apparent conductivity at a depth of 40 m.

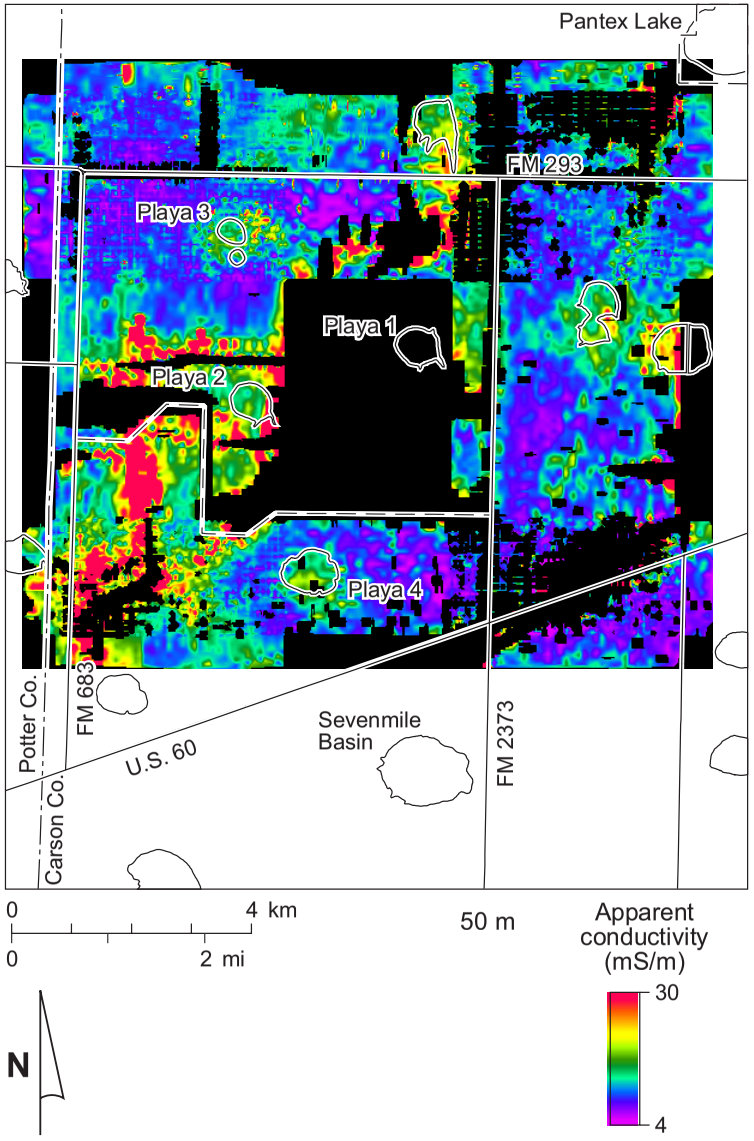

Figure B5. Apparent conductivity at a depth of 50 m.

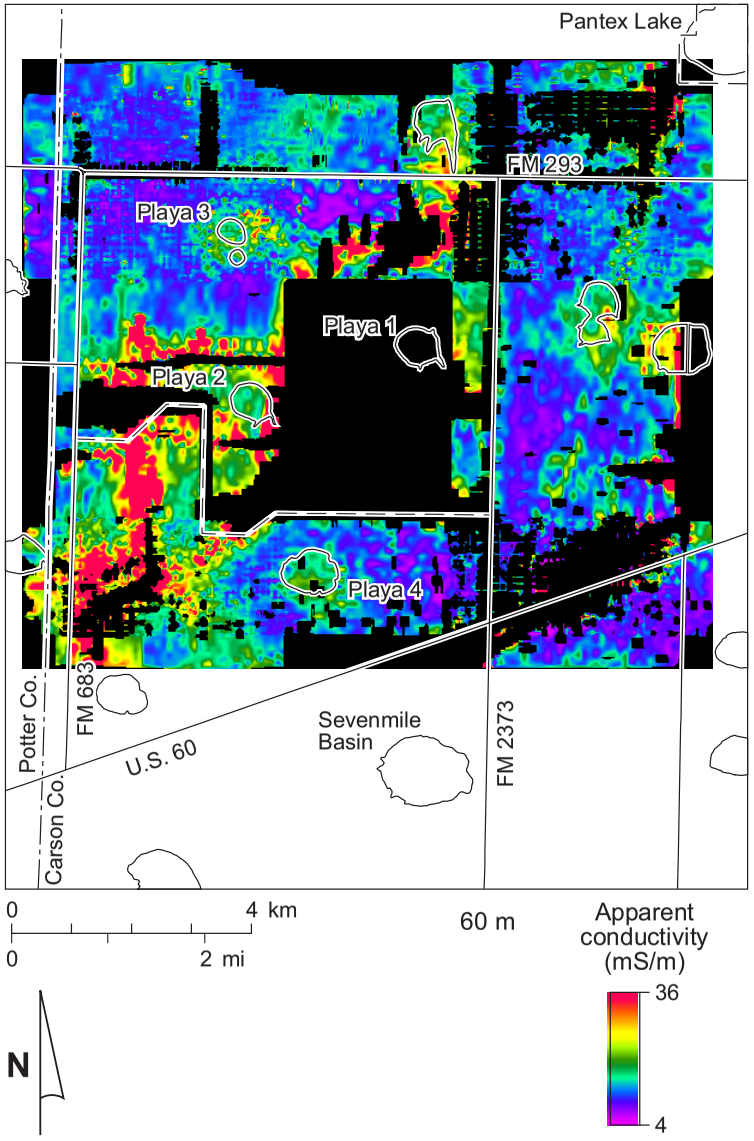

Figure B6. Apparent conductivity at a depth of 60 m.

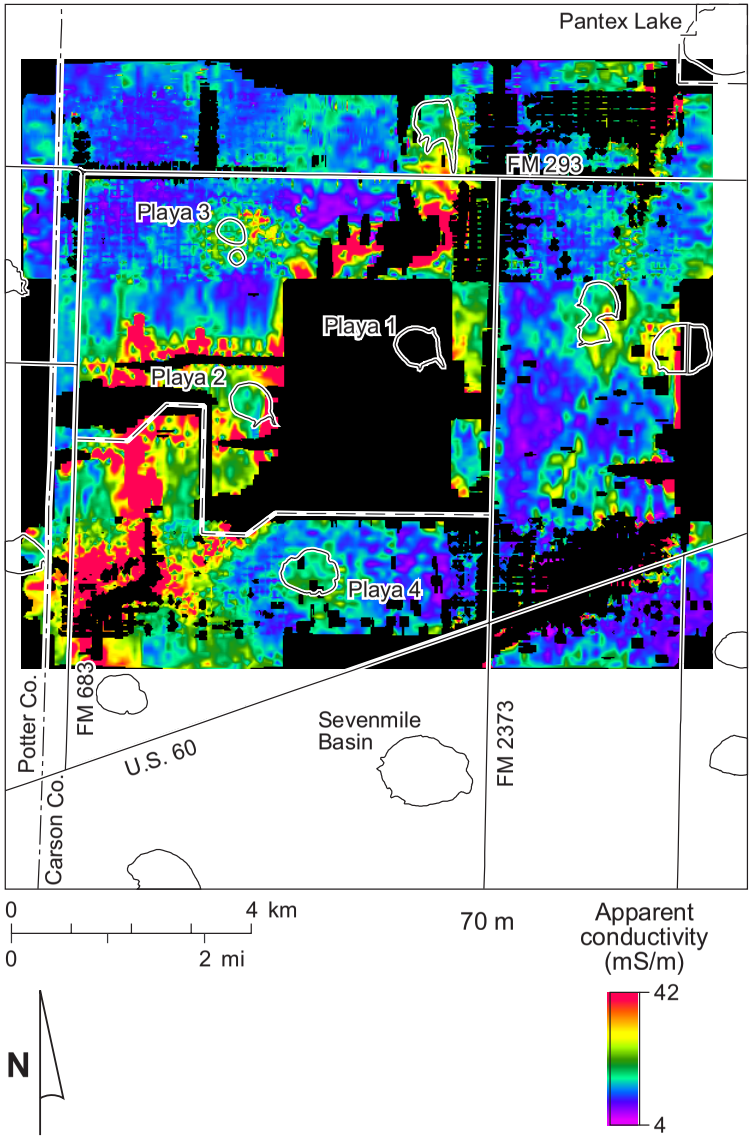

Figure B7. Apparent conductivity at a depth of 70 m.

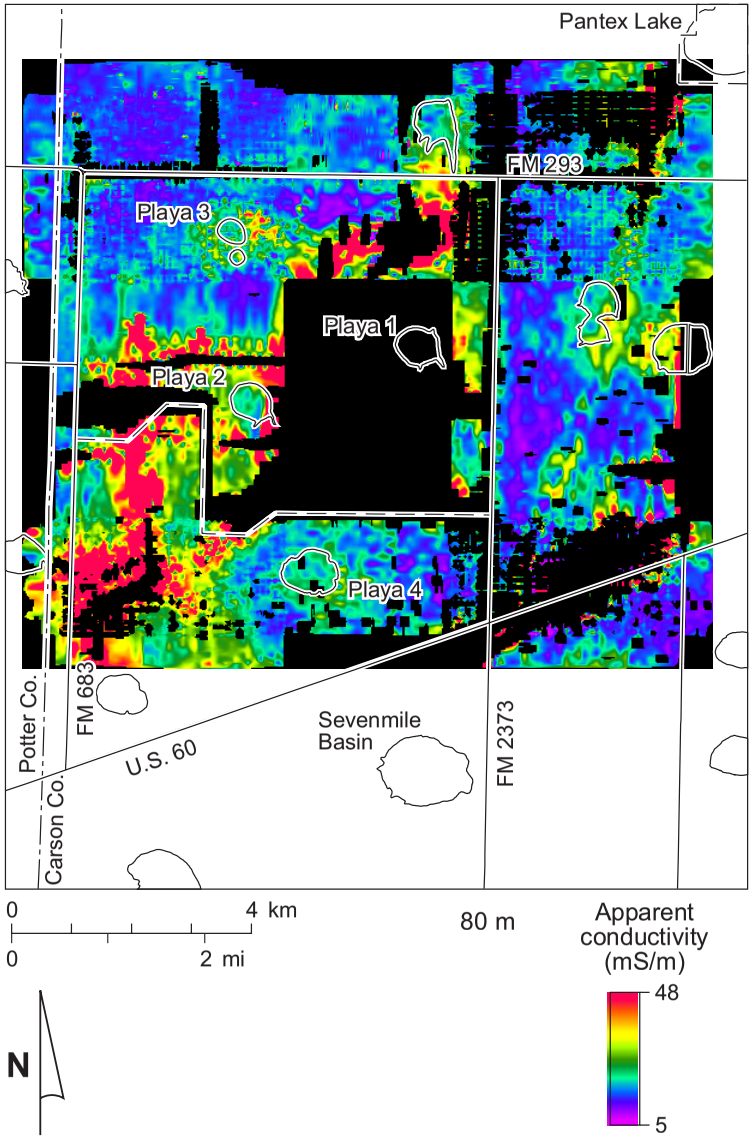

Figure B8. Apparent conductivity at a depth of 80 m

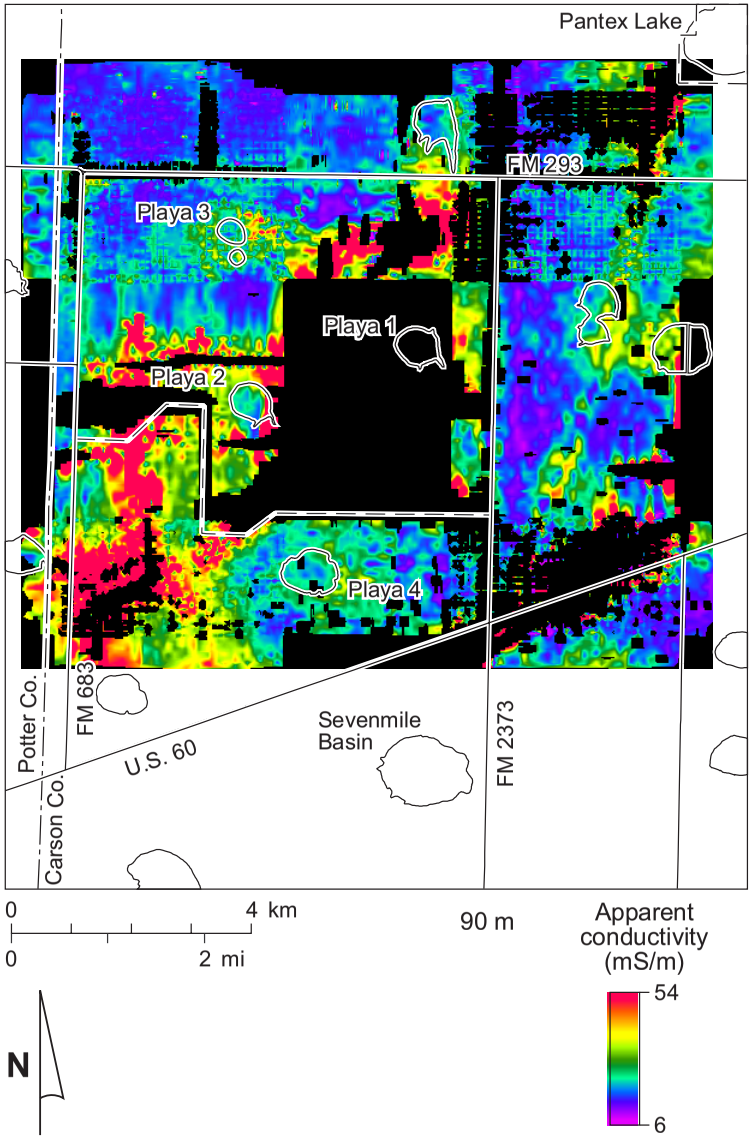

Figure B9. Apparent conductivity at a depth of 90 m.

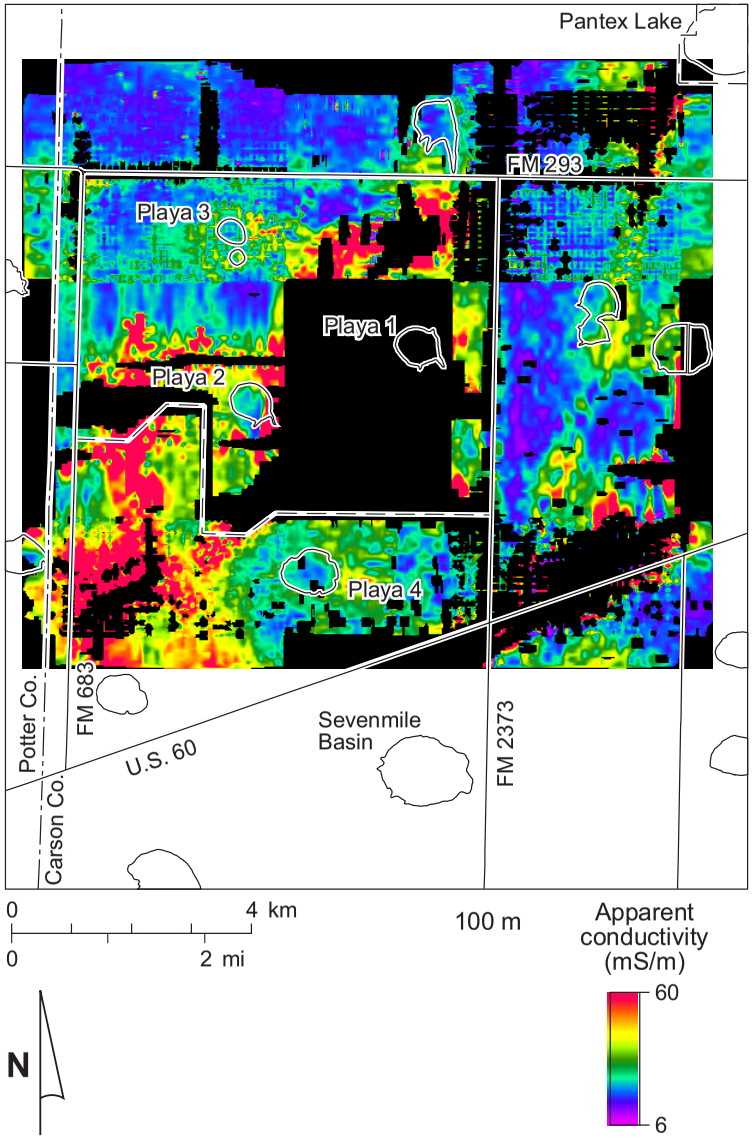

Figure B10. Apparent conductivity at a depth of 100 m.

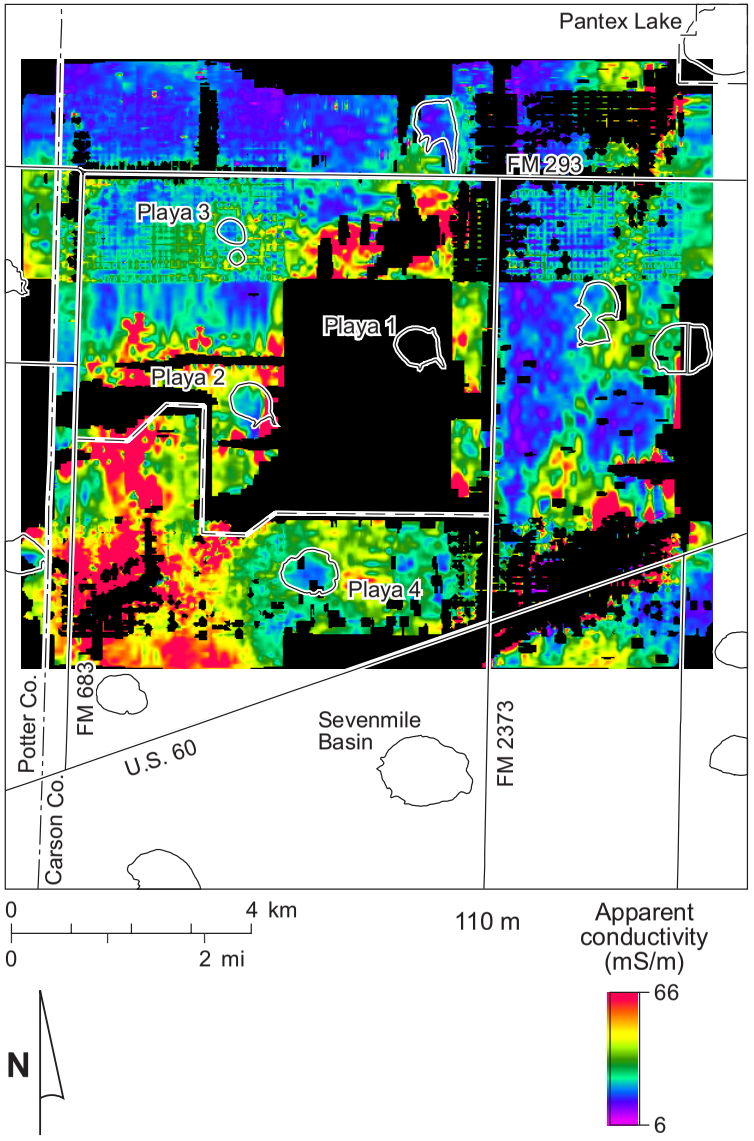

Figure B11. Apparent conductivity at a depth of 110 m.

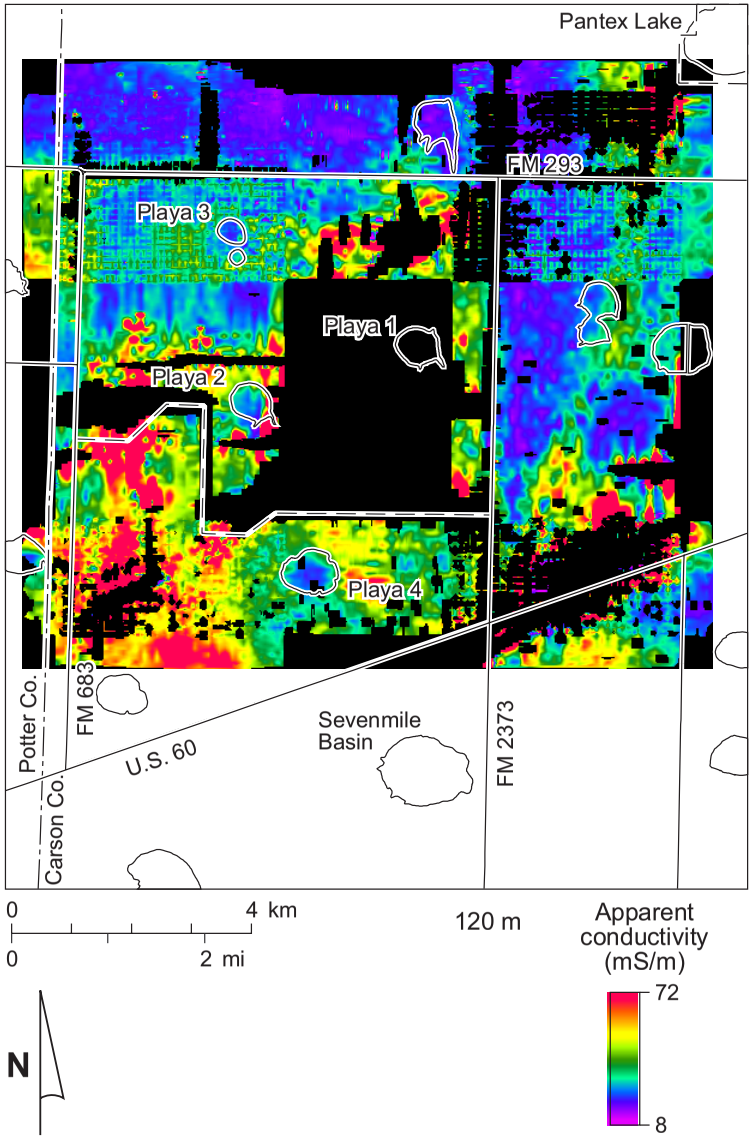

Figure B12. Apparent conductivity at a depth of 120 m.

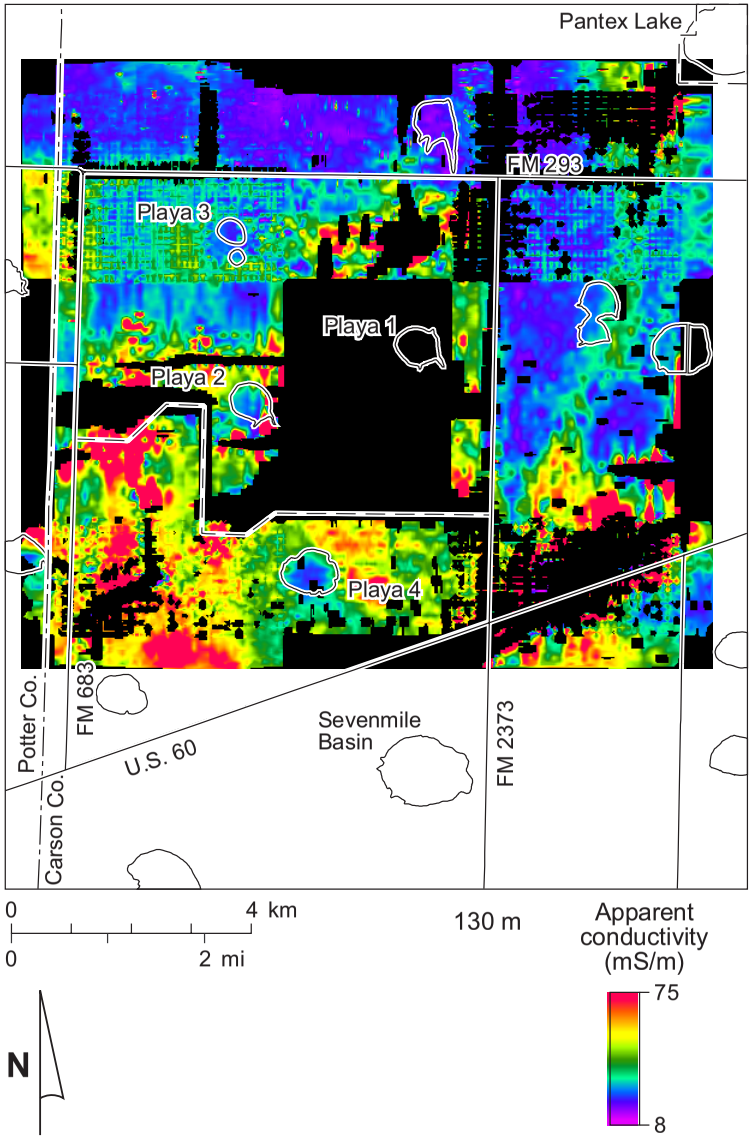

Figure B13. Apparent conductivity at a depth of 130 m.

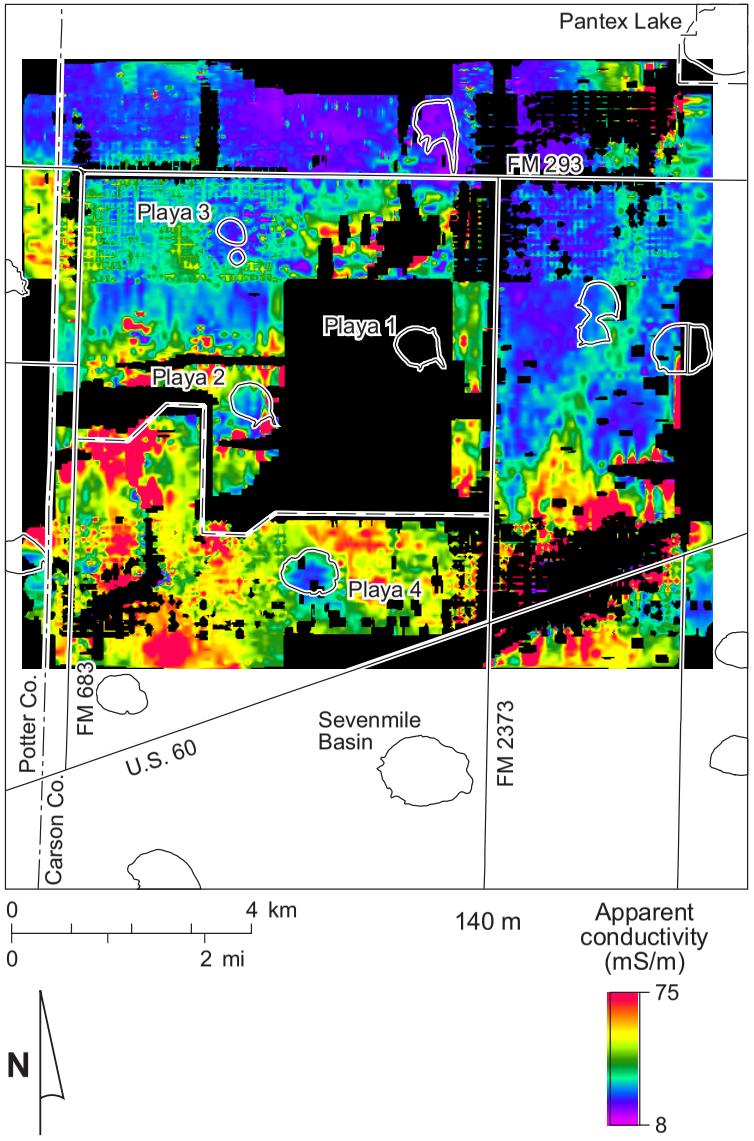

Figure B14. Apparent conductivity at a depth of 140 m.

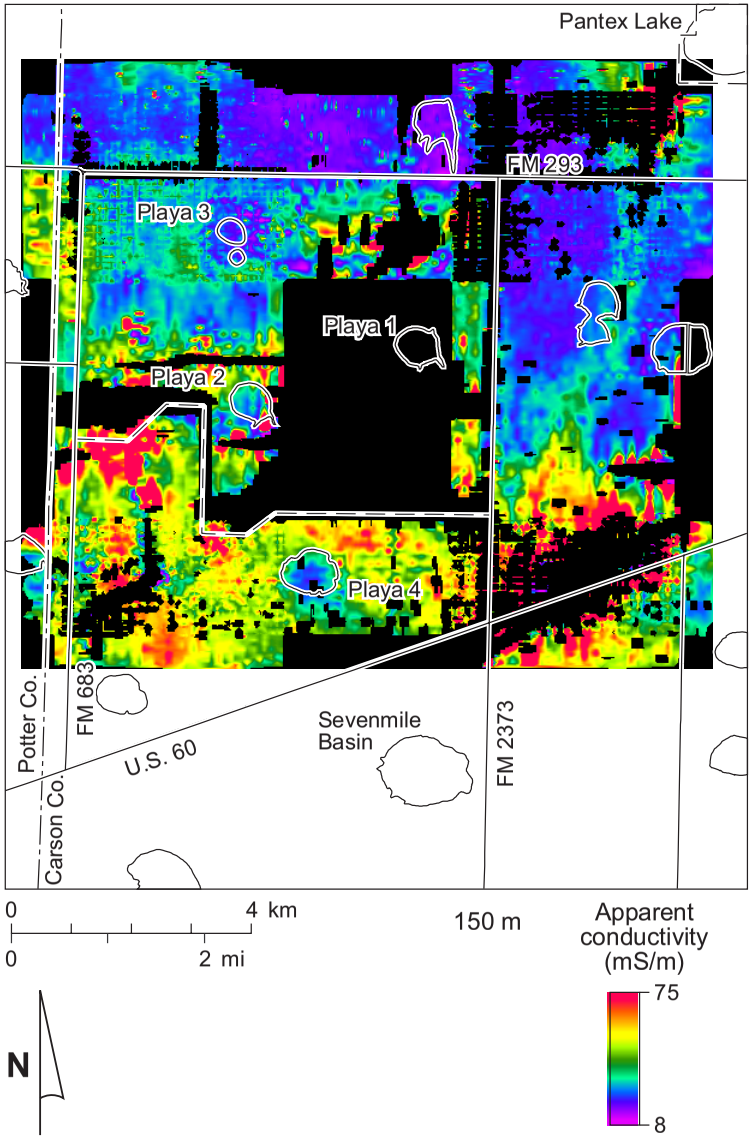

Figure B15. Apparent conductivity at a depth of 150 m.

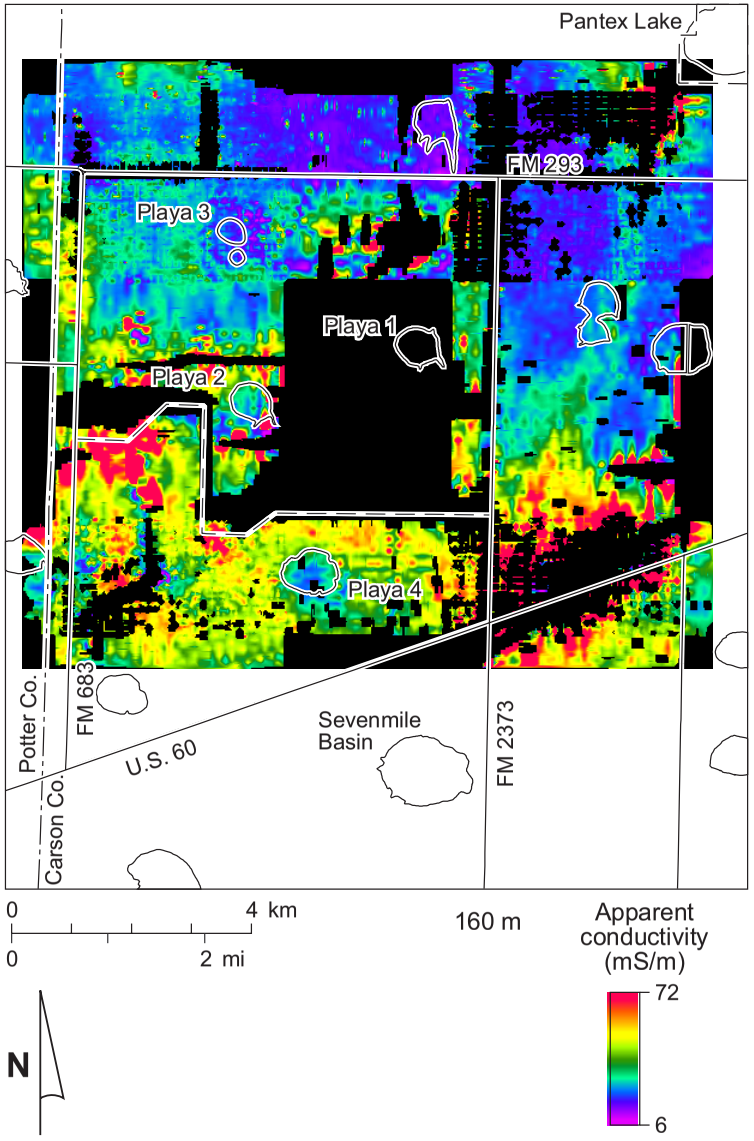

Figure B16. Apparent conductivity at a depth of 160 m.

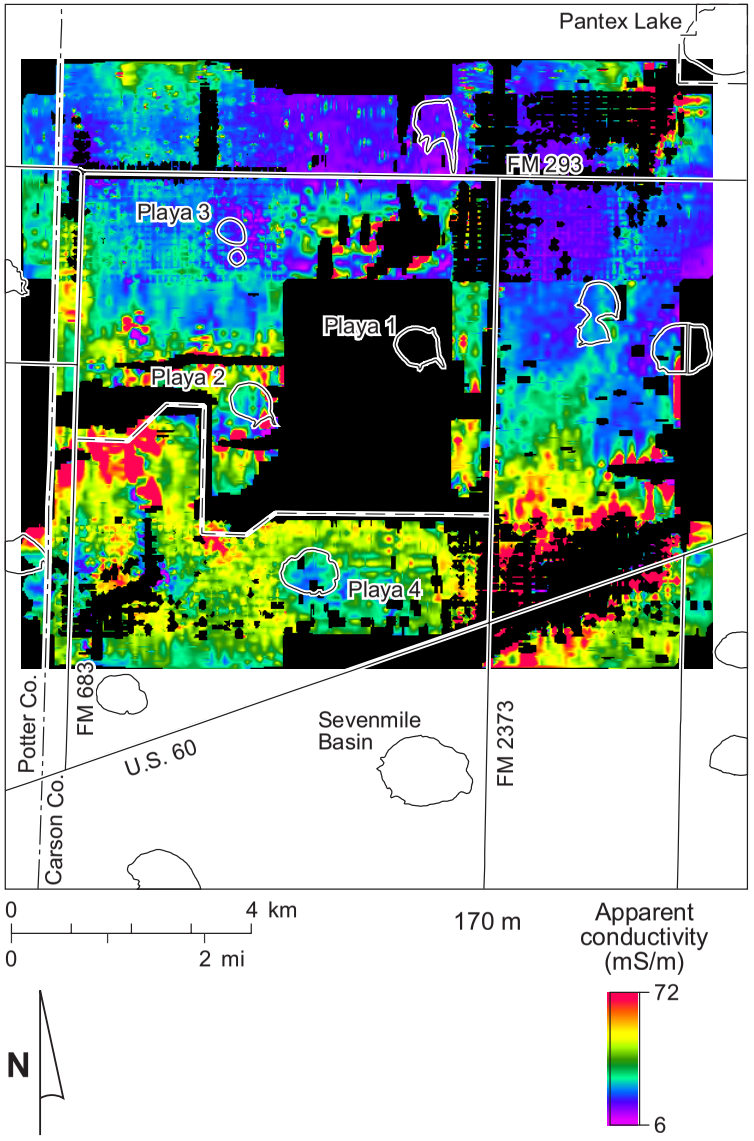

Figure B17. Apparent conductivity at a depth of 170 m.

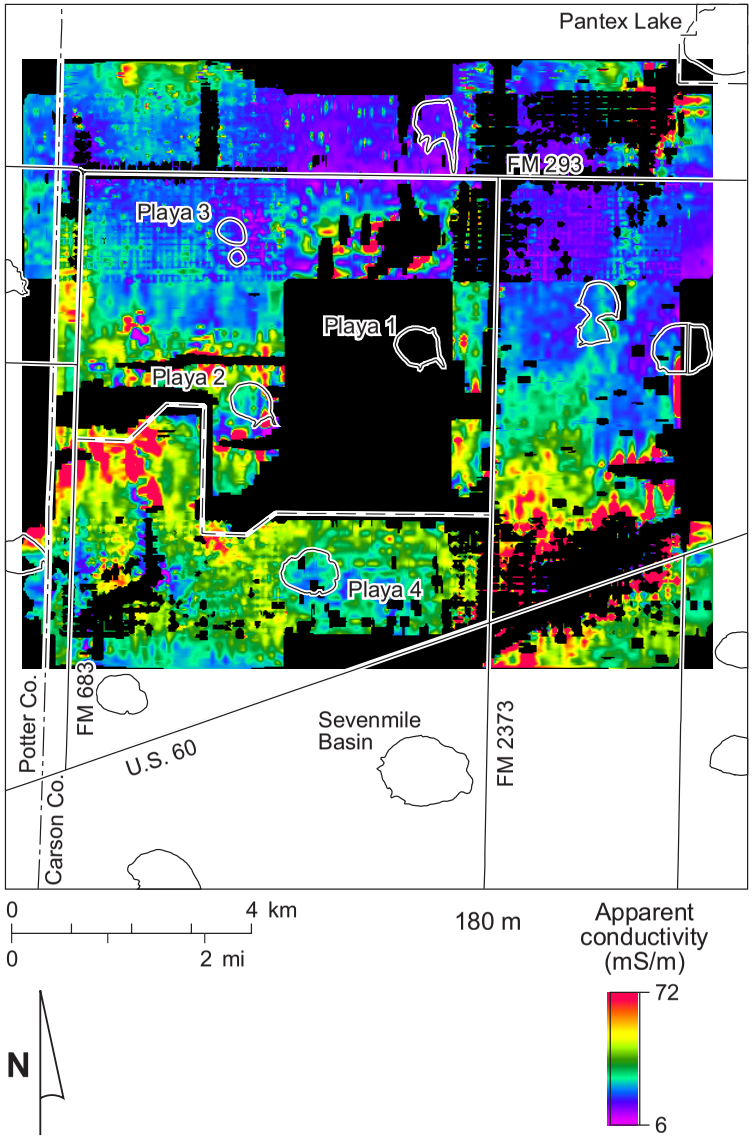

Figure B18. Apparent conductivity at a depth of 180 m.

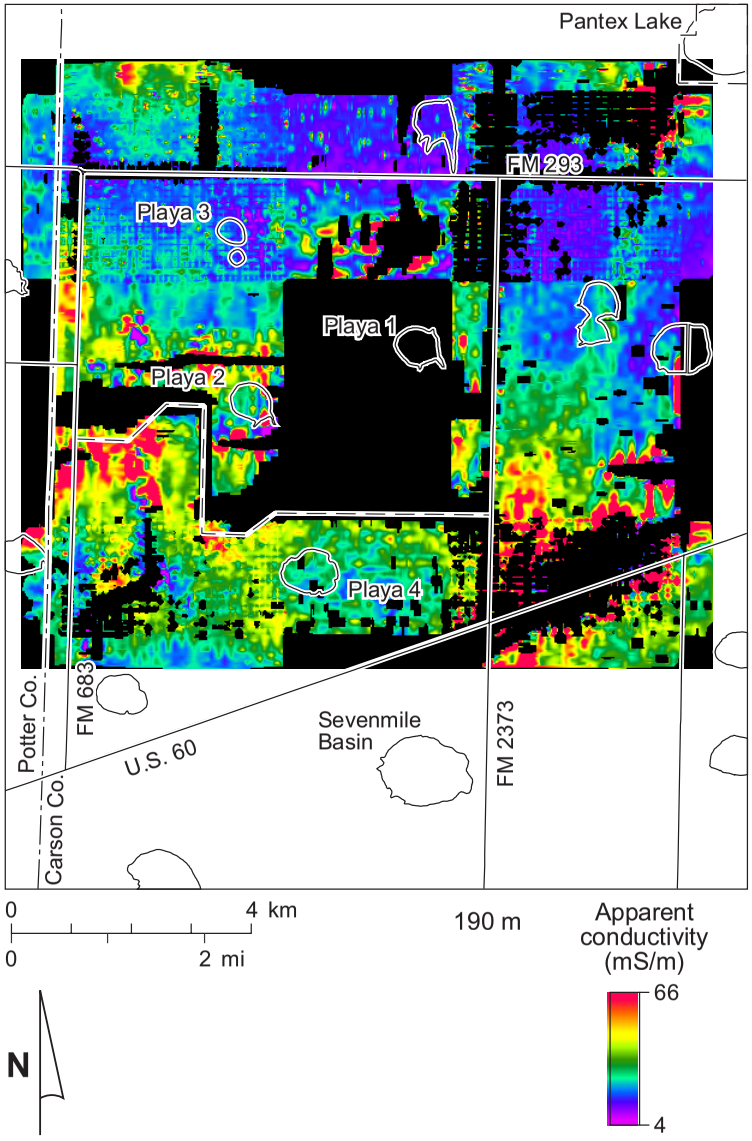

Figure B19. Apparent conductivity at a depth of 190 m.

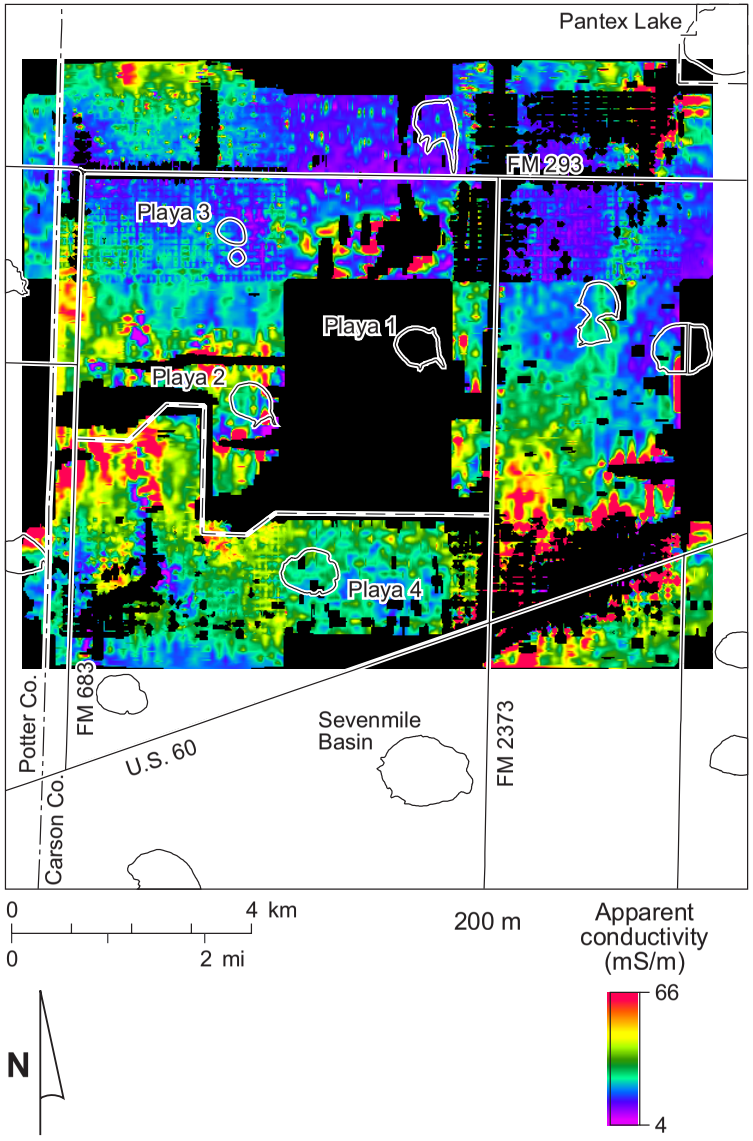

Figure B20. Apparent conductivity at a depth of 200 m.